iScience

CellPress
OPEN ACCESS

Article

Metallo-protease Peptidase M84 from *Bacillus altitudinis* induces ROS-dependent apoptosis in ovarian cancer cells by targeting PAR-1

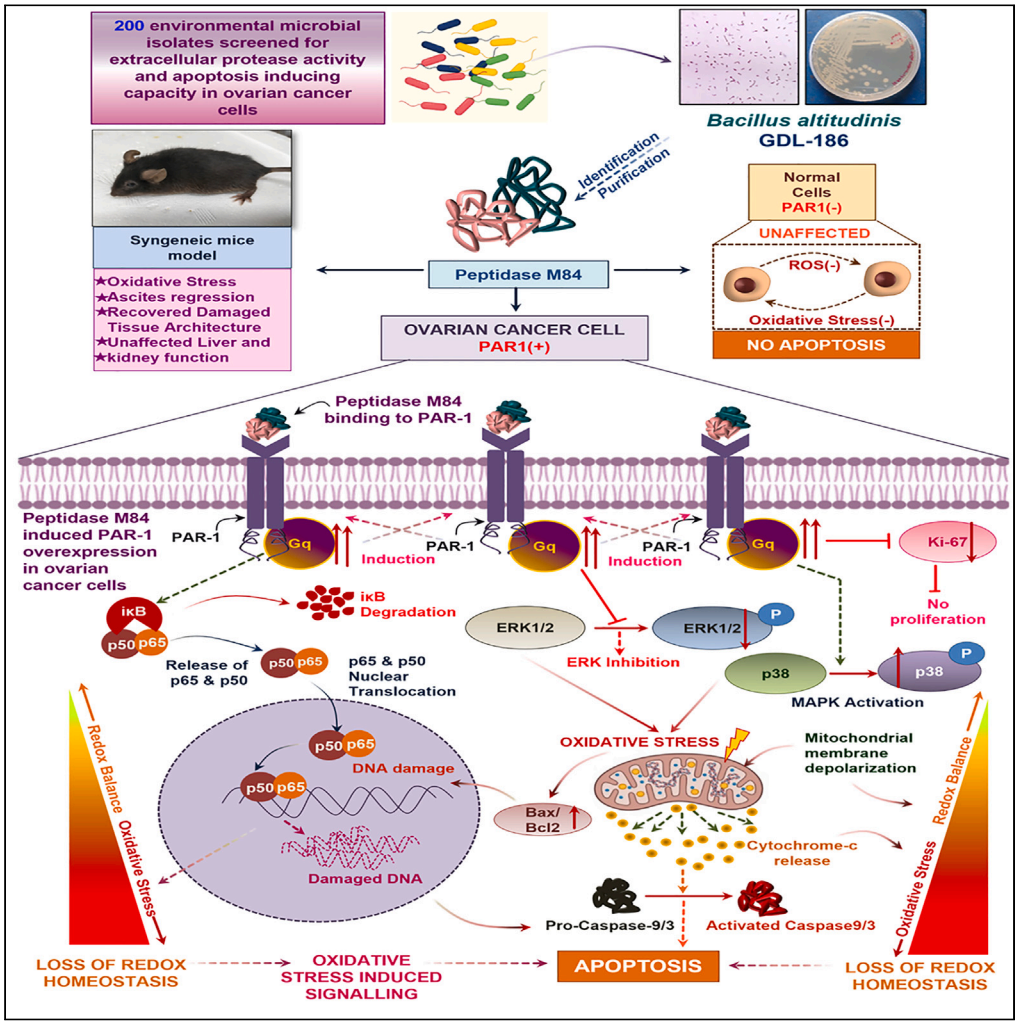

Niraj Nag, Tanusree Ray, Rima Tapader, ..., Ananda Pal, Parash Prasad, Amit Pal

palamit.app@gmail.com

Highlights

Bacillus altitudinis derived Peptidase M84 possesses anti-cancer properties

It triggered ROS-dependent apoptosis in PAR-1-positive ovarian cancer cells

PAR-1 negative normal healthy cells were unaffected with Peptidase M84 treatment

Peptidase M84 potentiated PAR-1 targeted ovarian cancer therapy

Nag et al., iScience *27*, 109828
June 21, 2024
https://doi.org/10.1016/j.isci.2024.109828

iScience

CellPress
OPEN ACCESS

Article

Metallo-protease Peptidase M84 from *Bacillus altitudinis* induces ROS-dependent apoptosis in ovarian cancer cells by targeting PAR-1

Niraj Nag,[1] Tanusree Ray,[1] Rima Tapader,[1] Animesh Gope,[2] Rajdeep Das,[3] Elizabeth Mahapatra,[4] Saibal Saha,[1] Ananda Pal,[2] Parash Prasad,[5] and Amit Pal[1,6,*]

SUMMARY

We have purified Peptidase M84 from *Bacillus altitudinis* in an effort to isolate anticancer proteases from environmental microbial isolates. This metallo-protease had no discernible impact on normal cell survival, but it specifically induced apoptosis in ovarian cancer cells. PAR-1, a GPCR which is reported to be overexpressed in ovarian cancer cells, was identified as a target of Peptidase M84. We observed that Peptidase M84 induced PAR-1 overexpression along with activating its downstream signaling effectors NF-κB and MAPK to promote excessive reactive oxygen species (ROS) generation. This evoked apoptotic death of the ovarian cancer cells through the intrinsic route. In *in vivo* set-up, weekly intraperitoneal administration of Peptidase M84 in syngeneic mice significantly diminished ascites accumulation, increasing murine survival rates by 60%. Collectively, our findings suggested that Peptidase M84 triggered PAR-1-mediated oxidative stress to act as an apoptosis inducer. This established Peptidase M84 as a drug candidate for receptor mediated targeted-therapy of ovarian cancer.

INTRODUCTION

In spite of remarkable improvements in chemotherapy regimens to treat ovarian cancer, it still remains one of the most lethal gynecological malignancies with a high recurrence and mortality rate.[1] Although cytoreductive surgery accompanied with platinum-based chemotherapy is the admissible treatment for epithelial ovarian cancer (EOC), the mortality rates have not improved markedly.[1–3] For instance, ovarian cancer is ranked eighth among the top ten common malignancies affecting Indian females as per Globocan 2018. Therefore, new therapies and alternative targets need to be developed to combat ovarian cancer.

In this regard, the anticancer potentials of natural products have been extensively explored for their differential effects as "cytoprotectors" to normal cells and "cytotoxics" to cancer cells. Predominantly, natural products exhibit this dual role by targeting several key molecules which in many instances impart resistance to conventional chemotherapy.[4–6] Herein, microorganisms supply structurally diverse natural products in abundance, serving the purpose of drug discovery. Extraction and purification of natural bacterial products are relatively cost-effective compared to chemically synthesized drugs.[7,8] Bacterial toxins and enzymes have been acknowledged for their anti-cancer effects. Reports are suggestive of their role as modulators of various cellular processes like apoptosis, differentiation, and proliferation. Bacterial products alone or when conjugated with other available anticancer drugs or irradiation can improve the efficiency of cancer therapy.[9–11] Didemnin B from *Tridemnum solidum* was among the earliest anti-cancer drugs of marine origin to enter clinical studies.[12] Similarly, Azurin from *Pseudomonas aeruginosa* and MakA from *Vibrio cholerae* have already shown promising anticancer effects.[13–15] Microbial proteases are reported to play their role through several mechanisms such as the inactivation of antimicrobial peptides,[16] disruption of the defensive mucosal barrier,[17] and elicitation of apoptosis in target cells.[18] For example, a protease obtained from *Serratia mercescens kums 3958* was reported to cause significant tumor regression when injected into solid tumors in BALB/c mice.[19,20] Previously, we have also reported bacterial subtilisin, a serine protease capable of potentiating apoptosis via ubiquitin mediated tubulin degradation pathway in breast cancer cells.[21] L-asparaginase (ASNase) is a pharmaceutically and clinically important microbial enzyme, isolated from different environmental sources that showed hopeful outcomes in cancer therapy as well.[22,23] Studies on extracellular metallo-protease arazyme from *Serratia proteamaculans* stated that it could

[1]Division of Molecular Pathophysiology, ICMR-National Institute of Cholera and Enteric Diseases (ICMR-NICED), P-33, CIT Road, Scheme-XM, Beliaghata, Kolkata, West Bengal 700010, India
[2]Division of Clinical Medicine, ICMR-National Institute of Cholera and Enteric Diseases (ICMR-NICED), P-33, CIT Road, Scheme-XM, Beliaghata, Kolkata, West Bengal 700010, India
[3]Molecular Cell Biology of Autophagy Lab, The Francis Crick Institute, 1, Midland Road, London NW1 1AT, UK
[4]Department of Environmental Carcinogenesis and Toxicology, Chittaranjan National Cancer Institute, 37, S.P. Mukherjee Road, Kolkata, West Bengal 700026, India
[5]Division of Experimental Hematology and Cancer Biology, Cincinnati Children's Hospital and Medical Center, 3333 Burnet Avenue, Cincinnati 45229-3026, OH, USA
[6]Lead contact
*Correspondence: palamit.app@gmail.com
https://doi.org/10.1016/j.isci.2024.109828

effectively inhibit metastatic murine melanoma via MMP-8 cross-reactive antibody stimulation.[24] These findings revealed a possible mechanism of cytotoxic action of microbial proteases on cancer cells.

Oxidative stress serves as a key modulator of signaling pathways involved in cellular survival and death depending on the cellular threshold levels of ROS. Dynamic redox homeostasis is thus a characteristic of exorbitantly growing cancer cells. Hence, most cytotoxic cancer drugs are observed to promote cell death by inducing oxidative stress, either directly or indirectly.[25,26] Higher levels of cellular reactive oxygen species (ROS) persuade mitochondria dependent conventional intrinsic pathway of apoptosis following caspase-9 activation.[26,27] Proteases can induce bio-signalling pathways and control cellular functions through the cleavage of protease-activated receptors (PARs), a notable G-protein coupled receptors (GPCRs).[28] The subtypes of PARs, ranging from PAR 1–4, have been found to be overexpressed in cancer cells with respect to healthy normal cells.[29] PARs play important roles in the apoptosis of cancer cells and carcinogenesis depending on the stimuli.[30–33] Studies demonstrated the differential expression pattern of PAR-1 in both transcriptional and translational levels in ovarian carcinoma tissue samples, while, negligible or none in the normal ovarian surface epithelium.[34] Moreover, PAR-1 agonists also showed apoptosis in intestinal epithelial cells.[35] Nevertheless, the molecular mechanism by which overexpression of PAR-1 can perturb the viability of cancer cells remains a less examined area of cancer research. PAR-1 activation can trigger ROS generation in cancer cells.[36,37] However, both PAR-1 and ROS are also reported to be associated with the activation of NF-κB and MAP kinases imparting apoptosis of cancer cells.[37,38] Therefore, PAR-1 mediated ROS targeting therapy using proteases may be proven to be advantageous to selectively kill cancer cells.

The objective of our study, therefore involved screening of environmental microbial isolates to identify a naturally occurring microbial protease with apoptosis capacitating potentials and deciphering its anticancer mechanism. In this study, we report that Peptidase M84, an extracellular metallo-protease purified from an environmental isolate of gram-positive *Bacillus altitudinis* can augment oxidative stress by altering PAR-1 activity to trigger apoptotic signaling in human and mice ovarian carcinoma cells with high selective toxicity. Our present study provides a deeper insight into the mechanism underlying Peptidase M84-induced apoptosis in ovarian cancer cells in a PAR-1/ROS-dependent manner which was not elucidated previously. Thus, Peptidase M84 may be employed for its chemotherapeutic efficacy in the future for ovarian cancer amelioration.

RESULTS

The culture supernatant from isolate GDL-186 which showed similarity with *Bacillus altitudinis*, triggered apoptosis in PA-1 cells

High extracellular protease activity was recorded for the 12 isolates (GDL-184, GDL-185, GDL-186, GDL-187, GDL-188, GDL-191, GDL-201, GDL-71, GDL-213, BSF-4, BSF-80, and BSF-32) screened out of 200 environmental isolates (Figures 1A and 1B). Initially, we assessed the apoptosis inducing potentials of the sterile supernatants extracted from these isolates among PA-1 cells by flow cytometry after treatment. Herein, PA-1 cells, specifically treated with GDL-186 supernatant underwent apoptosis significantly (Figures 1C and 1D). This was reconfirmed when the GDL-186 supernatant also successfully induced apoptosis in SKOV3 cells additionally. Contrarily, no apoptosis inductions were noted among both PA-1 and SKOV3 cells upon treatment with GDL-186 supernatant pre-incubated with EDTA and PMSF. A significant decrease in the percentage of apoptotic PA-1 and SKOV3 cells was enumerated, denoting protease mediated apoptosis inducing property of GDL-186 isolate (Figures S1A–S1D). Thereafter, we identified GDL-186 as a *Bacillus* species after deciphering 100% sequence homology of their 16S rRNA with that of *Bacillus altitudinis* strain in NCBI Blast results. The gene sequence was submitted to NCBI GenBank under accession number OP738003.1. (Figures S1E and S1F). We also confirmed the identity of the GDL-186 isolate based on DNA gyrase B sequence homology analysis (Figures S1G and S1H). In addition to this, some major biochemical, microbiological, and morphological studies further strengthened our observation of the isolate GDL-186. We observed no growth of this isolate in Macconkey agar plates containing crystal violet. Following this, the phenotypic results of this isolate showed medium-sized rod-shaped cells with aerobic growth, white to off-white-coloured moist colonies, motile and endospore-forming. This isolate was found as gram-positive bacilli also positive for oxidase and catalase. The biochemical profile illustrated that this isolate metabolizes D-arabinose, D-glucose, starch, fructose, and lactose. Other biochemical characterizations for indole, citrate utilization, triple sugar iron, lysine iron agar, and oxidative fermentation tests confirmed the environmental isolate as *Bacillus* sp. The identity of the isolate was definitively confirmed by whole genome sequencing, with the sequence deposited at DDBJ/ENA/GenBank under the accession JAZHFY000000000. All these results indicated that the isolate GDL-186 belonged to the Bacillus genus (Figures S2A–S2F, S3A, and S3B).

Purification and identification of secreted protease named Peptidase M84 from *Bacillus altitudinis* GDL-186

GDL-186 culture supernatant proteolytically degraded azocasein alongside inducing apoptosis in PA-1 cells. On this basis, we decided to purify and characterize this supernatant for its typical protease-like behavior. Firstly, EDTA and 1, 10- phenanthroline treatment inhibited the proteolytic activity of these crude supernatants which remained unaltered in PMSF and EGTA's presence. This hinted at GDL-186 being an extracellular zinc-dependent metallo-protease (Figures S4A and S4B). Next, the probable protease was concentrated following dialysis where the resultant non-binding and binding fractions were examined for proteolytic activity (Figures 2A and S4C) Interestingly, the non-binding fraction was observed to exhibit protease activity (Figure 2B). This was therefore pooled, concentrated, and analyzed by gel filtration (sephadex G-75). Two fractions (indicated as two different peaks in the chromatogram) were eluted from the G-75 column of which the first fraction showed higher protease activity compared to the second (Figures 2C and 2D). The first peak of sephadex G-75 elution was hence pooled, concentrated, and further analyzed in SDS-PAGE (15%). Two major bands around 25 kDa and 16 kDa molecular weights were distinctly observed which upon EDTA pre-incubation resulted in a single band at 25 kDa only (Figure 2E). This fraction of G-75 also showed single

A

No. of total bacterial isolates screened	No. of protease positive microbial isolates	No. of bacterial isolates for which protease activity was inhibited by EDTA	No. of bacterial isolates for which protease activity was inhibited by PMSF	No. of bacterial isolates induced apoptosis in cancer cells
200	12	7	4	1

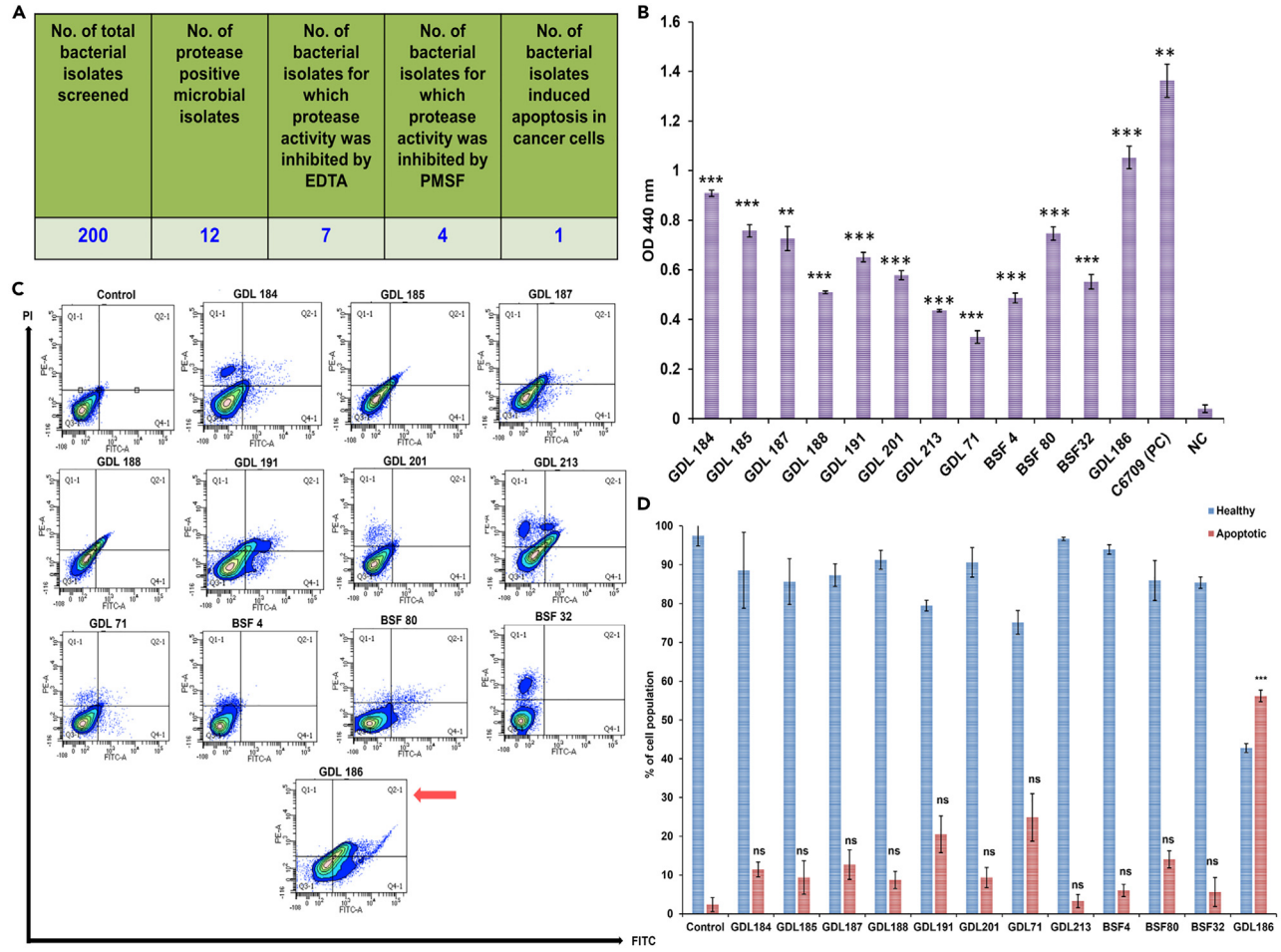

Figure 1. Screening of 200 bacterial isolates from environmental sources for extracellular protease activity and apoptosis inducing ability

(A) Results of azocasein assay are represented in tabular form (B) Results of azocasein assay are represented in graphical form. Culture supernatant of *Vibrio cholerae* EL Tor strain C6709 and nutrient broth were used as positive and negative controls, respectively.

(C) Annexin V/PI based flow-cytometric analysis to assess the apoptosis inducing ability of the culture supernatant of the protease-secreting isolates in PA-1 cells. In each display the lower right quadrant is for early apoptotic cells (Annexin V+/PI), the upper right is for late apoptotic cells (Annexin V+/PI+), the upper left is for necrotic population (Annexin V-/PI+) and lower left is for healthy cells (Annexin V-/PI-). The culture supernatant of GDL-186 isolate (marked with an arrow) shows significant apoptosis.

(D) The aforementioned results are graphically represented in the bar diagram. All statistical analysis was done by applying the Student's t test (unpaired two-tailed). Data are expressed in ±SEM. In all panels, (non-significant) ns $p > 0.05$, *$p \leq 0.05$, **$p \leq 0.01$, and ***$p \leq 0.001$. Error bars were calculated based on results obtained from a minimum of three independent experiments ($n = 3$). See also Figures S1–S3 and S13.

band in Native PAGE (10%) (Figure 2F). These bands were further characterized by nano-LC-MS/MS-TOF where the generated peptide sequence was homologous to "Peptidase M84" from *Bacillus altitudinis*. (Figure 2G). This enzyme typically consists of a consensus amino acid sequence HExxH and a Met-turn motif "CLMNY" in downstream of its active site. The histidines and glutamic acid act as zinc ligands and catalytic base, respectively.[39]

Inhibition of the protease activity revealed the metallo-protease nature of Peptidase M84 which was optimally active at normal physiological pH and temperature

Purified Peptidase M84 was also proteolytically active against azocasein. This activity was yet again inhibited by EDTA and 1,10- phenanthroline but remained unaltered with PMSF (Figure 2D). Inhibition studies once again confirmed that this purified Peptidase M84 was a zinc-containing metallo-protease. Additionally, native gelatin zymogram profile revealed Peptidase M84 to be proteolytically active against gelatin. A clear hollow zone due to gelatin degradation was attained in Native PAGE (with 0.1% gelatin) followed by Coomassie staining (Figure S4D). Peptidase M84 showed proteolytic activity over a wide range of pH values (from 4.0 to 11.0). Although, the optimal and the minimal activities of Peptidase M84 were recorded at pH 8.0 and pH 4.0, respectively, the enzyme kept 80–90% activity at pH 7.0–10.0 (Figure 2H). In line with

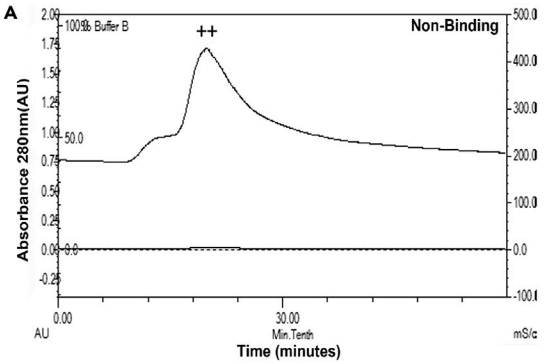
A
Non-Binding
++
Absorbance 280nm(AU)
Time (minutes)

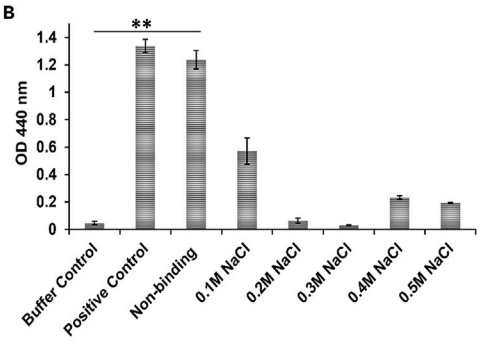
B
**
OD 440 nm
Buffer Control
Positive Control
Non-binding
0.1M NaCl
0.2M NaCl
0.3M NaCl
0.4M NaCl
0.5M NaCl

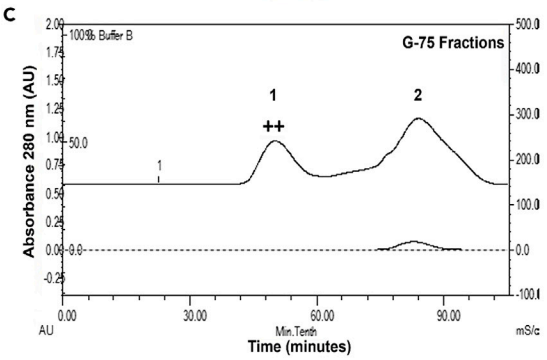
C
G-75 Fractions
1
2
++
Absorbance 280 nm (AU)
Time (minutes)

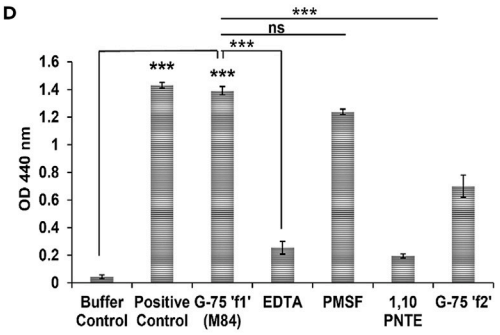
D
***
ns
***
OD 440 nm
Buffer Control
Positive Control
G-75 'f1' (M84)
EDTA
PMSF
1,10 PNTE
G-75 'f2'

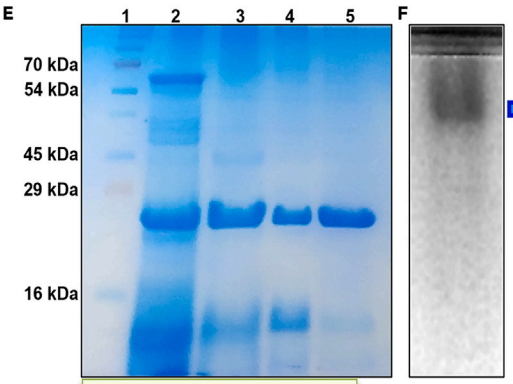
E
1 2 3 4 5
70 kDa
54 kDa
45 kDa
29 kDa
16 kDa
F
Lane 1: Marker
Lane 2: Crude
Lane 3: DE52 Non-binding
Lane 4: G75 Pool '1'
Lane 5: G75 Pool '1'+ EDTA

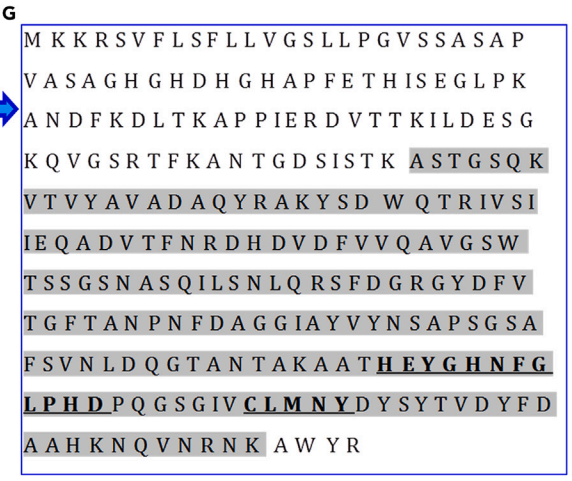
G
M K K R S V F L S F L L V G S L L P G V S S A S A P
V A S A G H G H D H G H A P F E T H I S E G L P K
A N D F K D L T K A P P I E R D V T T K I L D E S G
K Q V G S R T F K A N T G D S I S T K A S T G S Q K
V T V Y A V A D A Q Y R A K Y S D W Q T R I V S I
I E Q A D V T F N R D H D V D F V V Q A V G S W
T S S G S N A S Q I L S N L Q R S F D G R G Y D F V
T G F T A N P N F D A G G I A Y V Y N S A P S G S A
F S V N L D Q G T A N T A K A A T H E Y G H N F G
L P H D P Q G S G I V C L M N Y D Y S Y T V D Y F D
A A H K N Q V N R N K A W Y R

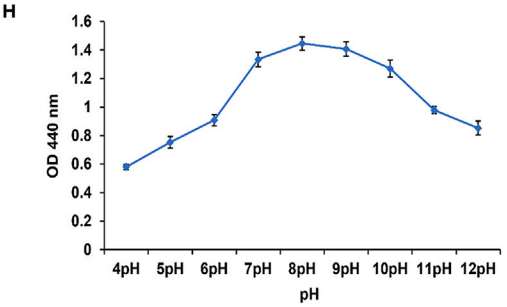
H
OD 440 nm
4pH 5pH 6pH 7pH 8pH 9pH 10pH 11pH 12pH
pH

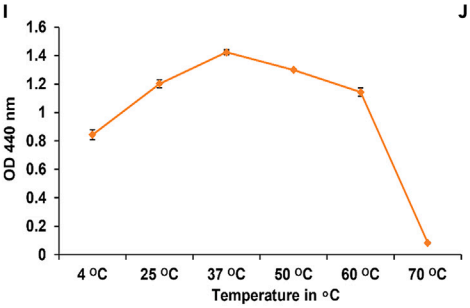
I
OD 440 nm
4 °C 25 °C 37 °C 50 °C 60 °C 70 °C
Temperature in °C

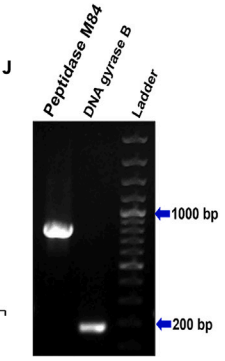
J
Peptidase M84
DNA gyrase B
Ladder
1000 bp
200 bp

Figure 2. Purification and identification of Peptidase M84 from *Bacillus altitudinis* GDL-186

(A) Chromatogram of DEAE-52 anion exchange chromatography of the ammonium sulfate precipitated crude protein fraction from GDL-186 culture supernatant.
(B) Azocasein assay with protein fractions (5.0 μg) obtained from DEAE-52 column shows higher protease activity in the non-binding fraction (++) as compared to the NaCl (0.1 M–0.5 M) eluted binding fractions.
(C) The chromatogram of the G-75 gel filtration chromatography shows separation of the non-binding fraction, represented as two individual peaks (G-75"f1" and G-75"f2").
(D) Azocasein assay with G-75 fractions shows maximum protease activity in the G-75 "f1" (++) fraction. This activity is inhibited by EDTA and 1,10-phenanthroline.
(E) 15% SDS-PAGE profile of the purified protease shows two major bands near 25 kDa and 16 kDa, which upon pre-incubation with EDTA shows a single band at 25 kDa.
(F) 12% Native-PAGE profile of the purified protease (G-75 "f1") shows a single band.
(G) Protein bands were identified by Nano-LC-MS/MS-TOF peptide sequencing which exhibited homology with "Peptidase M84". The peptides showing homology are with the background color. The active sites and the zinc-binding domains of the protease are underlined.
(H and I) Determination of the optimum pH and temperature of Peptidase M84.
(J) PCR amplification of the full-length (813bp) peptidase M84 gene (Lane 1) and DNA gyrase B gene (Lane 2) from *Bacillus altitudinis* strain GDL-186. All statistical analysis was done by applying Student's t test (two-tailed). Data are expressed in ±SEM. In all panels, ns $p > 0.05$, *$p \leq 0.05$, **$p \leq 0.01$, and ***$p \leq 0.001$. In each panel, error bars were calculated based on results obtained from a minimum of three independent experiments ($n = 3$). See also Figures S4 and S5.

this, Peptidase M84 exhibited maximum activity against azocasein at temperatures ranging from 37°C to 40°C which decreased gradually at 50°C–60°C. This protease showed suboptimal activity at temperatures ranging from 4°C to 25°C. At higher temperature (60°C–70°C), the proteolytic activity was almost completely abolished (Figure 2I).

We also evaluated the effect of Zn^{2+} on the azocaseinolytic activity of Peptidase M84. We observed that the Peptidase M84 protease activity was gradually increased with the Zn^{2+} concentration starting from 0.5 mM up to 2 mM. Interestingly, this activity was decreased in the presence of higher concentrations (5 mM and above) of Zn^{2+}. This activity was completely abolished by pre-treatment with EDTA or 1,10-phenanthroline. (Figures S4E and S4F) This can be explained by the binding of Zn^{2+} to non-catalytic ion-binding sites of metzincins, triggering a conformational change that results in the loss of proteolytic activity or by the precipitating effect induced by Zn^{2+}. Studies suggested that the addition of excess Zn^{2+} decreased the proteolytic activity of metzincins over the pH range from 7.0 to 9.0, pointing to this effect on $Zn(OH)_2$ precipitation on the protein.[40] Based on this, we can conclude the protease activity of Peptidase M84 is dependent on Zn^{2+}. Besides, the full-length amplified 813 bp gene encoded Peptidase M84 of *Bacillus altitudinis* was also detected in 0.8% agarose gel after PCR amplification (Figures 2J, S5A, and S5B). The molecular phylogenetic tree of Peptidase M84 derived from NCBI blast showed the distribution of the M84 metallo-proteases in Bacillus species (Figure S5C).

Peptidase M84 exhibited apoptosis and suppressed the proliferation of ovarian cancer cells but had no such impact on IOSE and PEMΦ cells

MTT cell viability assay showed a gradual depletion in the percentage of viable ovarian cancer cells with increasing concentrations of Peptidase M84, ranging between 0.5 μg/mL and 5.0 μg/mL. The *in vitro* safe dose (IC_{50}) of Peptidase M84 was found to be 2.0 μg/mL for PA-1 and SKOV3 cells. Furthermore, Peptidase M84 showed IC_{50} 3.0 μg/mL against ID8 cells (Figures S6A–S6C). These concentrations aligned with the concentrations used to detect apoptosis and study the bio-signalling pathways in the aforementioned cell lines.

Next, in order to investigate the cytotoxic effect of Peptidase M84, PA-1, SKOV3, and ID8 cells were treated with doses ranging between 1.0 μg/mL and 3.0 μg/mL for 18 h. Flow cytometry showed that Peptidase M84 caused significant apoptosis in these cell lines as compared to untreated cells. Inhibition of protease activity by EDTA showed a significant reduction in the percentage of apoptotic cells. However, this percentage was not affected by PMSF. These results clearly indicated that purified Peptidase M84 by virtue of its metalloprotease activity could promote cell death by inducing apoptosis in human and mouse ovarian cancer cells (Figures 3A–3D).

Ki-67 protein is considered as a proliferation marker for human tumor cells. Higher expression of nuclear Ki-67 is found in all stages of cell cycle not including the G0 stage and dead cells.[41] We noticed a lower abundance of Ki-67 in Peptidase M84 treated PA-1 and SKOV3 cells as compared to the untreated cells indicating that Peptidase M84 significantly restrained cancer cell proliferation. Contrarily, higher levels of nuclear Ki-67 in untreated control cells indicated rapid proliferation and increased survivability (Figures 3E–3G).

Peptidase M84 treatment also altered the morphology of PA-1 and SKOV3 cells. Peptidase M84 treatment showed a cell-distending effect at lower concentrations. A cell rounding effect was observed when cells were treated with increasing concentrations of Peptidase M84 for 18 h (Figure S6D).

During apoptosis, highly condensed inert and fragmented chromatin gets packaged into apoptotic bodies.[42] Herein, these became distinct upon Hoechst 33342 staining which indicated apoptotic induction. In Peptidase M84 treated PA-1, SKOV3, and ID8 cells, the percentage of condensed nuclei were 43.66, 38.33, and 44.33%, respectively, whereas the respective control cells were shown to be 13%, 10.6%, and 11.33% (Figures S6E and S6F). The result indicated that nuclei of Peptidase M84 treated cells exhibited condensed and bright nuclei while the untreated control cells showed less amount of condensed chromatin.

To understand the specificity, the effect of Peptidase M84 was evaluated on IOSE cells and PEMΦ cells in a similar range of doses of Peptidase M84. Almost all cells remained viable even at a concentration of 3.0 μg/mL of Peptidase M84. Therefore, Peptidase M84 selectively triggered apoptosis in malignant ovarian cells but not in normal cells (Figures 3H, 3I, S6G, and S6H). The respective gating patterns associated with these data are represented in Figure S13.

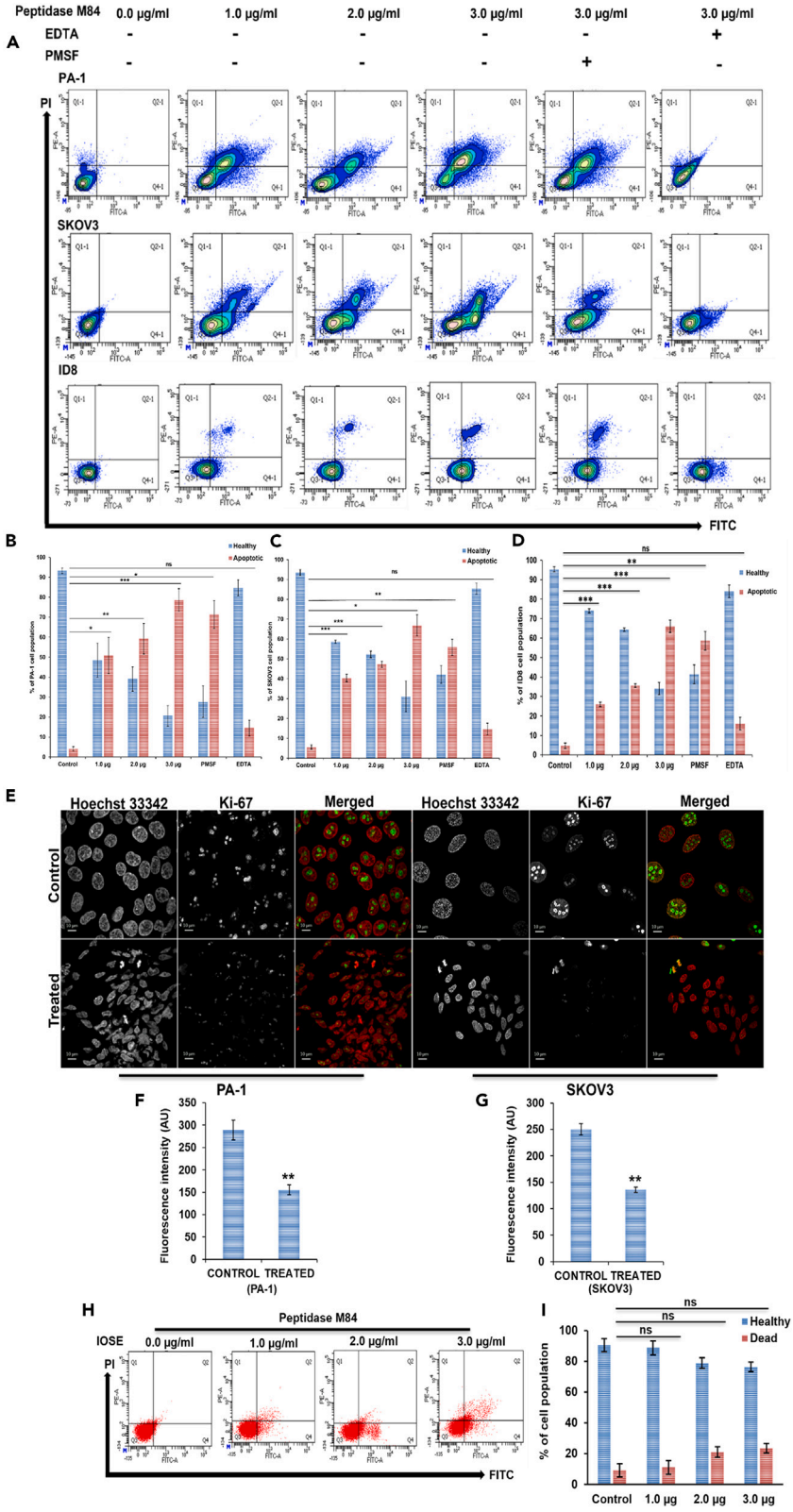
Peptidase M84
0.0 μg/ml
1.0 μg/ml
2.0 μg/ml
3.0 μg/ml
3.0 μg/ml
3.0 μg/ml
A
EDTA
PMSF
PA-1
PI
SKOV3
ID8
FITC
B
C
D
Healthy
Apoptotic
Control
1.0 μg
2.0 μg
3.0 μg
PMSF
EDTA
E
Hoechst 33342
Ki-67
Merged
Control
Treated
F
PA-1
Fluorescence intensity (AU)
CONTROL TREATED
(PA-1)
G
SKOV3
CONTROL TREATED
(SKOV3)
H
IOSE
I
Dead
% of cell population

Figure 3. Detection of cytotoxicity and apoptosis in Peptidase M84 treated ovarian cancer cells and human ovarian normal epithelial cells (IOSE) and in mouse peritoneal macrophage (PEMΦ) cells

(A) Flow cytometric analysis of Peptidase M84 treated PA1, SKOV3, and ID8 cells shows dose-dependent apoptosis. EDTA inhibition significantly reduces the effect while PMSF treatment does not affect cell viability.

(B–D) Bar diagrams show the percentage of healthy and apoptotic cell populations.

(E–G) Confocal imaging of nuclear Ki-67 (green) coupled with bar diagrams of mean fluorescence intensity (MFI) (calculated in Fiji) show a significant reduction in PA-1 and SKOV3 cell proliferation due to Peptidase M84 treatment.

(H and I) Flow cytometric analysis of the Peptidase M84 treated IOSE and PEMΦ cells shows no significant apoptosis as compared to the untreated cells. Bar diagrams of the data are also being presented. All statistical analysis was done by applying Student's t test (two-tailed). Data are expressed in ±SEM. In all panels, ns $p > 0.05$, *$p \leq 0.05$, **$p \leq 0.01$, and ***$p \leq 0.001$. In each panel, error bars were calculated based on results obtained from a minimum of three independent experiments ($n = 3$). Scale bars: 10 μm. See also Figures S6 and S13.

Peptidase M84 augmented ROS generation and activated the intrinsic canonical pathway of apoptosis in ovarian cancer cells

Excessive production of ROS overtakes the cellular antioxidant capacity. It results in oxidative stress, which ultimately contributes to the regulation of a wide range of signaling pathways and can impart oxidative damage mediated cell death.[43,44] The oxidative stress related to Peptidase M84 treatment was monitored by staining with DCFDA. Under the stimulation of ROS, DCFH is converted to fluorescent DCF upon oxidation. Peptidase M84 treatment showed an increase in ROS generation in PA-1, SKOV3, and ID8 cells, depicted as an increase in the mean fluorescence intensity level of DCF in comparison to untreated cells with time (6 h and 18 h). This could lead to initiating apoptotic signals (Figures 4A, 4B, S7A, and S7B). In contrast, Peptidase M84 failed to promote ROS generation in IOSE cells (Figures 4C–4E).

JC-1 dye uptake pattern suggested that Peptidase M84 also caused alterations in mitochondrial membrane potential ($\Delta\Psi$m) in PA-1 and SKOV3 cells. A decrease in $\Delta\Psi$m is considered as a major hallmark of apoptosis.[45] An increase in the ratio of green fluorescence to red fluorescence intensity levels clearly indicated disrupted $\Delta\Psi$m in Peptidase M84 treated cells in a time-dependent manner (6 h and 18 h) as compared to the untreated control cells (Figures 4F and 4G).

Herein, comet assay was performed to detect DNA damage in PA-1 and SKOV3 cells as a result of Peptidase M84 treatment as genotoxicity tests predominantly contribute to cancer research. We observed that Peptidase M84 treatment for 18 h gave a prominent induction of comet tail moment in ovarian cancer cells with respect to control untreated cells (Figures S7C–S7E).

Next, we examined the quantitative expression profiles of some prime regulatory proteins to study the possible molecular mechanism of apoptotic cascade induced by Peptidase M84. We observed that Peptidase M84 treatment resulted in the down-regulation of anti-apoptotic Bcl-2 levels and upregulation of pro-apoptotic marker Bax in PA-1 and SKOV3 cells concerning the untreated cells. Our results also revealed activation of caspase 9 and caspase 3 and upregulation of cleaved PARP expression levels by Peptidase M84. However, a consistent profile of caspase 8 expression levels indicated non-involvement of extrinsic (FADD-Caspase 8) apoptosis pathway in response to Peptidase M84 treatment in these cells (Figures 4H and 4I). Interestingly, no activation of caspase 3 was observed in Peptidase M84 treated normal IOSE cells (Figures S7F and S7G).

Mitochondrial cytochrome *c* functions as an electron carrier in the respiratory chain,[46] translocates to the cytosol in Peptidase M84 treated cells undergoing apoptosis, where it participates in the activation of specific caspases. We found an increase in the cytochrome *c* expression levels in cytosolic fraction devoid of mitochondria in translational levels in Peptidase M84 treated PA-1 and SKOV3 cells compared to the untreated cells. Densitometric data showed that the increase was highly significant. (Figures 4J and 4K).

Immunofluorescence data also supported this observation. Damaged mitochondria due to Peptidase M84 treatment were observed with mitotracker green FM staining. We also noticed a depletion in green fluorescence intensity levels in these cells. There was a reduction in co-localization between cytochrome *c* and mitochondria in PA-1 and SKOV3 cells treated with Peptidase M84 as compared to the untreated cells. Released cytochrome *c* was found to be distributed in punctate (red) form throughout the cytosol and around the nucleus of cells. Pearson's co-efficient values showed a significant reduction in co-localization between mitochondria and cytochrome *c* in Peptidase M84 treated PA-1 and SKOV3 cells (Figures 4L–4N).

Taken together, our findings implicated the activation of the intrinsic pathway of apoptosis in ovarian cancer cells by Peptidase M84 from *B. altitudinis*.

Peptidase M84 specifically interacted with PAR-1 and caused overexpression of PAR-1 in human and mouse ovarian cancer cells however not in human healthy ovarian epithelial cells

Real-time PCR data represented overexpression of PAR-1 in PA-1 and SKOV3 cells. We found almost 4-fold and 7-fold upregulation of PAR-1 mRNA levels in PA-1 and SKOV3 cells, respectively, as compared to the other PARs. (Figure 5A).

A time-dependent (6 h and 18 h) overexpression of PAR-1 was observed in PA-1 and SKOV3 cells after Peptidase M84 treatment (Figure 5B). Immunoblots also confirmed almost 2-fold increase in PAR-1 expression levels in PA-1 and SKOV3 cells and nearly 3.5-fold overexpression in ID8 cells after Peptidase M84 treatment (18 h) (Figures 5C and 5D). Importantly, no significant change was observed in the PAR-1 expression in IOSE cells (Figures 5C and 5D). Almost no expression of PAR-1 was observed in IOSE cells. Densitometric scan analysis depicted the intensity differences between PAR-1 expression levels in Peptidase M84 treated and untreated cells (Figure 5D). Immunofluorescence imaging also showed a significant increase in PAR-1 expression due to Peptidase M84 treatment in PA-1 and SKOV3 cells (Figures 5E–5H). This supports the fact that Peptidase M84 is unable to induce apoptosis in normal cells via effective modulation of PAR-1.

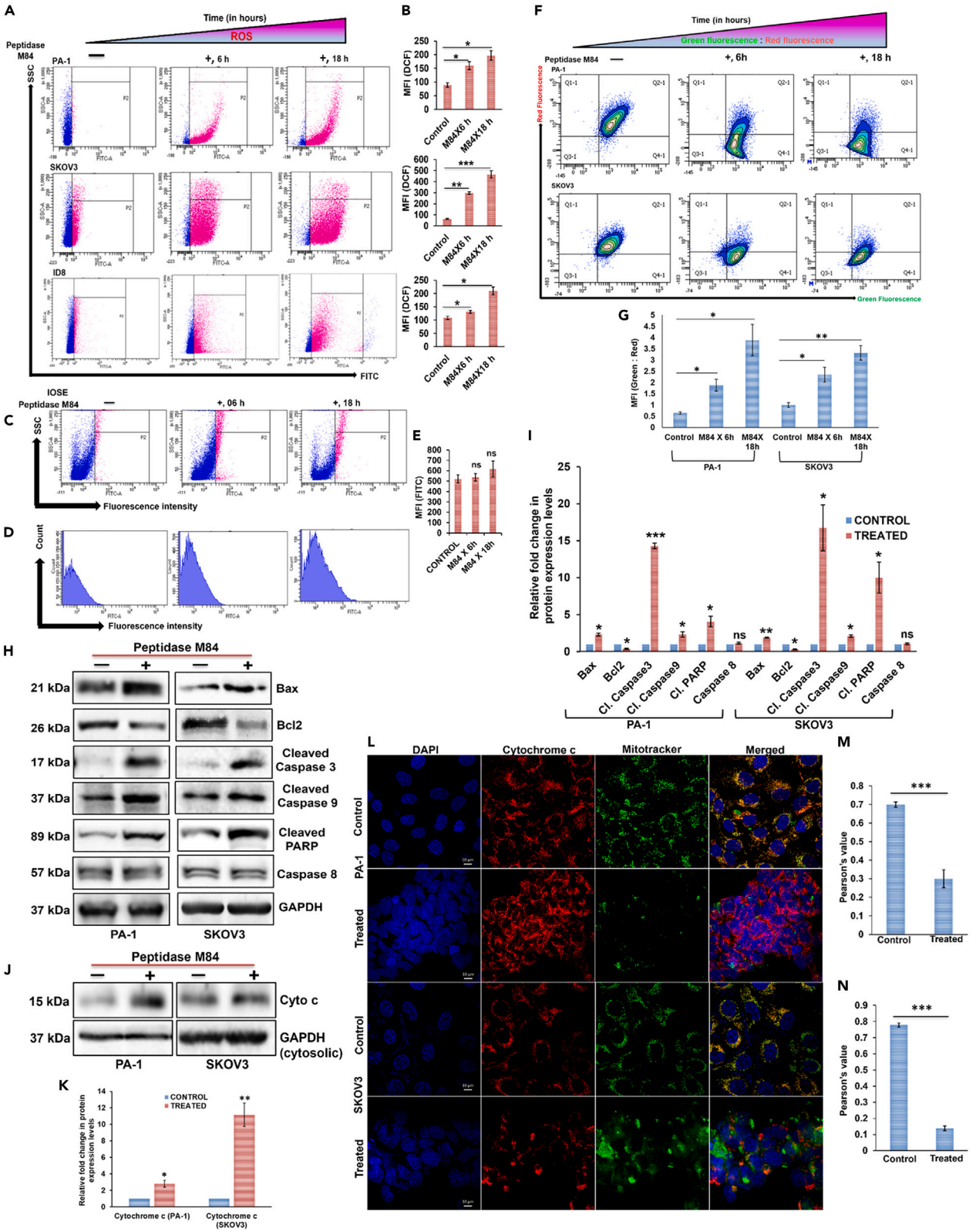
A
Time (in hours)
ROS
Peptidase M84
PA-1
+, 6 h
+, 18 h
SKOV3
ID8
SSC
FITC
B
MFI (DCF)
Control
M84X6 h
M84X18 h
C
IOSE
Peptidase M84
+, 06 h
+, 18 h
Fluorescence intensity
D
Count
Fluorescence intensity
E
MFI (FITC)
CONTROL
M84 X 6h
M84 X 18h
ns
F
Time (in hours)
Green fluorescence : Red fluorescence
Peptidase M84
+, 6h
+, 18 h
Red Fluorescence
Green Fluorescence
G
MFI (Green : Red)
Control
M84 X 6h
M84X 18h
PA-1
SKOV3
I
Relative fold change in protein expression levels
CONTROL
TREATED
Bax
Bcl2
Cl. Caspase3
Cl. Caspase9
Cl. PARP
Caspase 8
H
Peptidase M84
21 kDa
Bax
26 kDa
Bcl2
17 kDa
Cleaved Caspase 3
37 kDa
Cleaved Caspase 9
89 kDa
Cleaved PARP
57 kDa
Caspase 8
37 kDa
GAPDH
PA-1
SKOV3
J
Peptidase M84
15 kDa
Cyto c
37 kDa
GAPDH (cytosolic)
PA-1
SKOV3
K
Relative fold change in protein expression levels
CONTROL
TREATED
Cytochrome c (PA-1)
Cytochrome c (SKOV3)
L
DAPI
Cytochrome c
Mitotracker
Merged
Control
Treated
PA-1
SKOV3
M
Pearson's value
Control
Treated
N
Pearson's value
Control
Treated

Figure 4. Ovarian cancer cells undergo ROS-dependent intrinsic pathway due to Peptidase M84 treatment

(A) A time-dependent ROS generation was examined by DCFDA staining in PA-1, SKOV3, and ID8 cells after Peptidase M84 treatment. Quadrant "P2" represents cells producing ROS.

(B) Bar diagrams represent the MFI of DCF.

(C and D) Detection of ROS generation in normal IOSE cells after Peptidase M84 treatment by DCFDA staining. No significant ROS generation is found even after 18 h of treatment.

(E) Bar diagram of mean fluorescence intensity of DCF is represented.

(F and G) JC-1 staining data with bar diagrams of MFI (green: red) show the disruption of mitochondrial membrane potential with time in Peptidase M84 treated PA-1 and SKOV3 cells. Cell population positive for green fluorescence signified disrupted mitochondrial membrane potential.

(H and I) The immunoblots represent expression levels of major proteins of the intrinsic apoptotic pathway in Peptidase M84 induced and un-induced PA-1 and SKOV3 cells. Densitometric analysis for relative protein expression is plotted as a histogram.

(J and K) Immunoblot with bar diagram of densitometry scan of cytochrome *c* in the mitochondria-free cytosolic fraction in Peptidase M84 treated PA-1 and SKOV3 cells depict the release of cytochrome *c* from mitochondria.

(L–N) Immunofluorescence along with bar diagrams of Pearson's co-efficient values show a reduction in co-localization between mitochondria (green) and cytochrome *c* (red) due to Peptidase M84 treatment in PA-1 and SKOV3 cells. In each panel, error bars were calculated based on results obtained from a minimum of three independent experiments. All statistical analysis was done by applying Student's t test (two-tailed). Data are expressed in ±SEM. In all panels, ns $p > 0.05$, *$p \leq 0.05$, **$p \leq 0.01$, and ***$p \leq 0.001$. Scale bars: 10 μm. Densitometric analysis was performed on ImageJ and Gel Quant softwares. Band intensities were normalized to loading controls GAPDH. Pearson's co-efficient was calculated in Fiji (https://imagej.net/software/fiji/). See also Figures S7 and S13.

Next, we proceeded with immunoprecipitation to identify the receptor of Peptidase M84 and to elucidate the physical interaction between them. The outcome revealed Peptidase M84 specifically bound and interacted with PAR-1 when PA-1 and SKOV3 cells. A band of PAR-1 (50 kDa) was observed in western blot when PAR-1 was immunoprecipitated with Peptidase M84 specific antisera (Figure 5I). Additionally, bands of Peptidase M84 (25 kDa and 16 kDa) were also observed when Peptidase M84 was immunoprecipitated with anti-PAR-1 antibody (Figure 5J). In this context, another western blot with the raised antisera against Peptidase M84 showed two major bands at 25 kDa and 16 kDa. These bands were similar to that in 15% SDS-PAGE profile of purified Peptidase M84 (Figure S7H). Furthermore, binding and interaction between Peptidase M84 and PAR-1 were also validated by co-localization based confocal imaging. An increase in Pearson's co-efficient values in Peptidase M84 treated (30 min) PA-1 and SKOV3 cells as compared to untreated cells indicated the possible interaction between PAR-1 and Peptidase M84 (Figures 5K–5M, S8A, and S8B).

Peptidase M84 persuaded PAR-1 dependent apoptosis in ovarian cancer cells by triggering NF-κB and MAPK signaling mediated ROS generation

Thrombin-mediated PAR-1 activation generally regulates major signaling pathways such as p38 MAPK and NF-κB which ultimately triggers further ROS generation.[47–49] Likewise, in this study immunoblots of cytosolic and nuclear fractions of PA-1 and SKOV3 cells showed Peptidase M84 treatment promoted nuclear translocation p50 and p65 proteins, suggesting the activation of NF-κB signaling. We observed significant expression of p50 and p65 proteins in the nuclear fraction of Peptidase M84 treated cells as compared to untreated cells. Densitometry represented the ratio of protein expression between nucleus to cytosol of Peptidase M84 induced and un-induced cells. Histone H3 (nuclear protein) and alpha-tubulin (cytosolic protein) were used as loading controls (Figures 6A and 6B) Immunofluorescence imaging of Peptidase M84 treated and untreated cells further supported our findings and showed prominent nuclear translocation of the same proteins. There was an increase in the ratio of nuclear to cytosolic mean fluorescence intensity of p50 and p65 proteins in Peptidase M84 treated cells (Figures 6C–6G).

Immunofluorescence also indicated the overall increase of phospho-p38 (p-p38) expression levels in Peptidase M84 treated cells (Figures S9A–S9C). Results obtained from immunoblot also depicted the level of p–p38 and phospho-ERK1/2 was significantly increased and decreased respectively due to Peptidase M84 treatment. However, the entire cellular p38 and ERK1/2 levels remained unaltered. Thus, our report revealed that Peptidase M84 also modulated MAP kinase pathways in ovarian cancer cells (Figures 6H and 6I).

We aimed to decipher whether the interaction between Peptidase M84 and PAR-1 directly persuaded apoptotic signaling in ovarian cancer cells. Peptidase M84 treatment on PA-1 and SKOV3 cells showed cellular apoptosis. When these cells were priorly treated with PAR-1 inhibitor (ML161) followed by Peptidase M84 treatment for 18 h, there was an absence of apoptosis. Furthermore, knockdown of PAR-1 was achieved by si-RNA transfection for 48 h in PA-1 and SKOV3 cells (Figures S9D and S9E). These PAR-1 silenced cells behaved like untreated cells even after Peptidase M84 treatment. Hence, our data illustrated that Peptidase M84-induced apoptosis in ovarian cancer cells in a PAR-1 dependent manner (Figures 6J–6L).

We found that Peptidase M84 augmented ROS levels in ovarian cancer via activation of MAP kinase and NF-κB. To confirm whether these signaling pathways were directly responsible for cellular apoptosis, PA-1 and SKOV3 cells were pre-incubated with either NF-κB inhibitor (MG132) or p38 inhibitor (SB203580) or both followed by Peptidase M84 treatment for 18 h. When cells were pre-incubated with MG132 only 58% of PA-1 and 49% of SKOV3 cells showed apoptosis. Cells pre-incubated with SB203580 only 51% of PA-1 and 41% of SKOV3 cells showed apoptosis. Importantly, the majority of the cells undergoing apoptosis under the aforementioned conditions were mostly in the early apoptotic phase. Interestingly, when both inhibitors were applied together no significant apoptosis was noticed. Furthermore, no significant apoptosis was noticed when cells were incubated with ROS quencher (NAC) prior to protease treatment. This observation suggested the major involvement of ROS in Peptidase M84 induced apoptosis in ovarian cancer cells (Figures 6J–6L). We noticed that ML161 pre-treatment inhibited the Peptidase M84 mediated nuclear translocation of p50 and p65 (Figure S10A). Immunoblot also confirmed that Peptidase

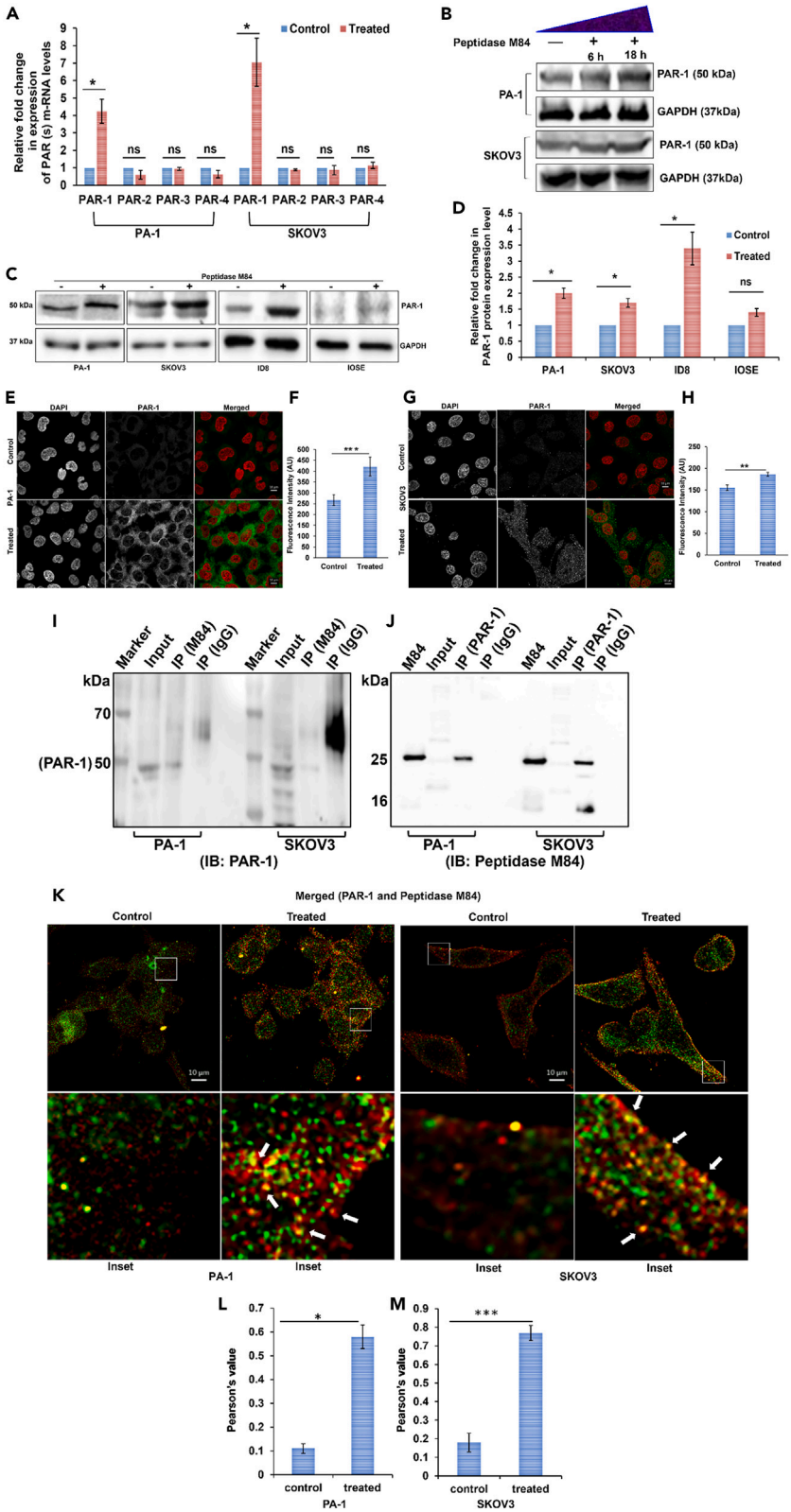
A
Relative fold change in expression of PAR (s) m-RNA levels
Control
Treated
PAR-1 PAR-2 PAR-3 PAR-4 PAR-1 PAR-2 PAR-3 PAR-4
PA-1
SKOV3
B
Peptidase M84
6 h
18 h
PA-1
PAR-1 (50 kDa)
GAPDH (37kDa)
SKOV3
PAR-1 (50 kDa)
GAPDH (37kDa)
C
Peptidase M84
50 kDa
37 kDa
PAR-1
GAPDH
PA-1
SKOV3
ID8
IOSE
D
Relative fold change in PAR-1 protein expression level
Control
Treated
PA-1
SKOV3
ID8
IOSE
E
DAPI
PAR-1
Merged
Control
PA-1
Treated
F
Fluorescence Intensity (AU)
Control
Treated
G
DAPI
PAR-1
Merged
Control
SKOV3
Treated
H
Fluorescence Intensity (AU)
Control
Treated
I
Marker
Input
IP (M84)
IP (IgG)
kDa
70
(PAR-1) 50
PA-1
SKOV3
(IB: PAR-1)
J
M84
Input
IP (PAR-1)
IP (IgG)
kDa
25
16
PA-1
SKOV3
(IB: Peptidase M84)
K
Merged (PAR-1 and Peptidase M84)
Control
Treated
Inset
PA-1
SKOV3
L
Pearson's value
control
treated
PA-1
M
Pearson's value
control
treated
SKOV3

Figure 5. Peptidase M84 persuaded apoptosis in ovarian cancer cells by modulating PAR-1

(A) Real-time PCR analysis of *PAR-1*, *PAR-2*, *PAR3*, *and PAR-4* genes in Peptidase M84 treated and untreated PA1 and SKOV3 cells. Ct values are normalized to *GAPDH* expression, and 2^{-ddct} values are calculated ($n = 3$).

(B) Western blot shows a time-dependent increase in PAR-1 expression levels in Peptidase M84 treated PA-1 and SKOV3 cells.

(C and D) Western blot together with bar diagram of densitometry scan of PAR-1 expression in Peptidase M84 treated (18 h) and untreated PA-1, SKOV3, ID8, and IOSE cells.

(E–H) Confocal imaging with respective bar diagrams of MFI of PAR-1 expression levels (green) in PA-1 and SKOV3 cells.

(I) Co-immunoprecipitation study of PAR-1 and Peptidase M84 reveals the interaction between PAR-1 and Peptidase M84 in both PA-1 and SKOV3 cells. Here, whole-cell lysates (WCL) from these cells were loaded as inputs.

(J) Bands of Peptidase M84 are observed in IB when Peptidase M84 was immunoprecipitated with PAR-1. Here, purified Peptidase M84 from *B. altitudinis* was loaded as input.

(K) Confocal imaging revealed co-localization between Peptidase M84 (green) and PAR-1(red) in Peptidase M84 treated PA-1 and SKOV3 cells.

(L and M) Bar diagrams showed Pearson's co-efficient values. In each panel, error bars were calculated based on results obtained from a minimum of three independent experiments. All statistical analysis was done by applying the Student's t test (two-tailed). In all panels, ns $p > 0.05$, *$p \leq 0.05$, **$p \leq 0.01$, and ***$p \leq 0.001$. Data are expressed in ±SEM. Scale bars: 10 μm. Densitometric analysis was performed on ImageJ and Gel Quant softwares. Band intensities were normalized to loading controls GAPDH. Pearson's co-efficient was calculated in Fiji (https://imagej.net/software/fiji/). See also Figures S7 and S8.

M84 induced phosphorylation of p38 was inhibited by ML161 pre-treatment in PA-1 cells. However, the total p38 concentration remained consistent (Figure S10B). Therefore, Peptidase M84 mediated NF-κB and MAP kinase pathways were regulated by PAR-1 activity alterations.

We have stated earlier that Peptidase M84 treatment promoted ROS generation in ovarian cancer cells. Interestingly, cells pre-treated with ML-161 displayed no significant ROS generation even after Peptidase M84 treatment for 18 h. Inhibition studies with MG132 and SB203580 further strengthened that blockade of NF-κB and p38 either individually or together impaired further ROS production in ovarian cancer cells (Figures S11A–S11C). Hence, Peptidase M84 induced PAR-1 dependent activation of both NF-κB and p38 to enhance ROS levels in ovarian cancer cells. Taken together our data illustrated that Peptidase M84 induced apoptosis by effectively targeting PAR-1 in accordance with the specific involvement of p38, NF-κB, and ROS.

Peptidase M84 treatment improved the survival of ID8 bearing mice and impeded body weight increase due to ascites accumulation and also affected the viability of ID8 cells *in vivo*

Tumor was induced intraperitoneally with ID8 cells (5×10^6) and the survival rate and the alterations in body weight were observed in C57BL/6 mice (Figure 7A). In the ID8 control mice, the rate of survival was 60% after 30 days and 10% after 60 days. When 3.0 μg/mL Peptidase M84 was injected at a weekly interval for 7 successive weeks the rate of survival was increased to 90% after 30 days and 70% after 60 days (Figure 7B). The body weight of ID8 control group enhanced from 25 g (0 days) to 45 g (after 60 days of tumor inoculation). On the other hand, in Peptidase M84 treated group and buffer control group no significant alterations in body weight were noticed (Figures 7C, S12A, and S12B). Inactivated Peptidase M84 (EDTA treated) failed to ameliorate the survival rate of ID8 induced mice and also showed an increase in body weight (Figure 7C).

In addition, viable ID8 cells were evaluated by trypan blue staining. At the inception of this investigation ID8 cells (5×10^6) were inoculated in the peritoneum cavity of mice and there was a gradual proliferation of viable ID8 cells in tumor control group. Peptidase M84 treatment caused a significant decline in the count of viable ID8 cells after 45^{th} and 60^{th} days. Peptidase M84 inactivated by EDTA did not affect the viability of ID8 cells at all (Figures 7D and 7E). Altogether our findings elucidated that the antitumour property of Peptidase M84 was linked to its proteolytic activity.

Peptidase M84 augmented oxidative stress in mice

To evaluate the Peptidase M84 mediated oxidative stress, biochemical tests were performed with different phase II detoxifying enzymes and LPO in the serum samples of mice. The level of LPO in serum is considered a marker for cellular oxidative stress. After 45 days of treatment, the number of viable ID8 cells significantly lessened in group-3 as compared to group-2 and the level of LPO in the serum was also found to be lowered in group-3 than to that of tumor control group-2. This indicated that Peptidase M84 itself could induce oxidative stress. After 45 days of Peptidase M84 treatment, the LPO level in group-3 was at normal levels as compared to group-1. The LPO levels of group-4 were found similar to group-2 after 45 days of treatment (Figure 7F).

The levels of catalase, SOD, and GSH in serum were relatively low because of excessive oxidative stress. After 45 days of Peptidase M84 treatment, the number of viable ID8 cells significantly declined in group-3 compared to group-2 and an increase in the levels of these enzymes was found in group-3 than to group-2. In addition to the aforementioned observations, the levels of catalase, GSH, and SOD in serum of group-4 were noticed as similar to group-2 after 45 days of treatment. Interestingly, there was no significant difference observed in any of the aforementioned biochemical markers when normal animals were treated with Peptidase M84 (group-6) (Figures 7G–7I). These observations clearly pointed out that Peptidase M84 triggered apoptosis in ID8 cells via oxidative stress-mediated damage.

Studies based on the biochemical index of the liver and kidney of mice revealed peptidase M84 did not cause any significant toxicity

To observe any adverse effects of exposure to Peptidase M84, a chronic toxicity study for 45 days was also been performed on experimental C57BL/6 mice. Alterations in the level of biochemical parameters, such as SGOT (AST), SGPT (ALT) (parameters for drug-induced liver injury),

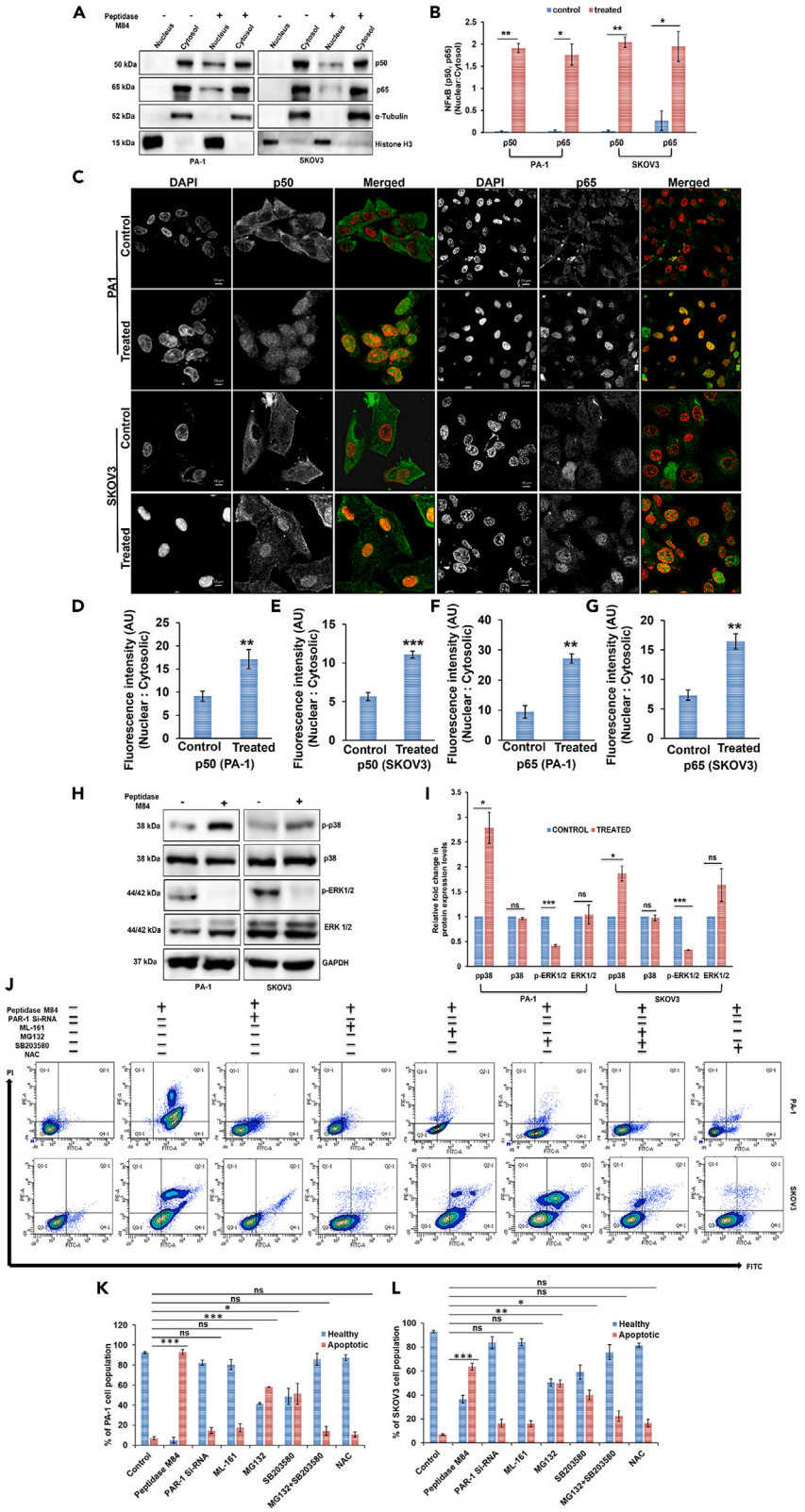
A
Peptidase M84
Nucleus
Cytosol
50 kDa
65 kDa
52 kDa
15 kDa
p50
p65
α-Tubulin
Histone H3
PA-1
SKOV3
B
control
treated
NF-κB (p50, p65) (Nuclear/Cytosol)
p50
p65
PA-1
SKOV3
C
DAPI
p50
Merged
p65
PA1
SKOV3
Control
Treated
D
Fluorescence intensity (AU) (Nuclear : Cytosolic)
p50 (PA-1)
E
p50 (SKOV3)
F
p65 (PA-1)
G
p65 (SKOV3)
H
38 kDa
44/42 kDa
37 kDa
p-p38
p38
p-ERK1/2
ERK 1/2
GAPDH
I
CONTROL
TREATED
Relative fold change in protein expression levels
pp38
p-ERK1/2
ERK1/2
J
Peptidase M84
PAR-1 Si-RNA
ML-161
MG132
SB203580
NAC
PI
FITC
PA-1
SKOV3
K
% of PA-1 cell population
Healthy
Apoptotic
Control
Peptidase M84
PAR-1 Si-RNA
ML-161
MG132
SB203580
MG132+SB203580
NAC
L
% of SKOV3 cell population

Figure 6. Peptidase M84 triggers PAR-1 induced apoptosis in ovarian cancer cells via NF-κB, MAPK, and ROS-dependent manner

(A and B) Western blot and bar diagram of densitometric scan (nucleus: cytosol) indicate enhanced nuclear translocation of p50 and p65 after Peptidase M84 treatment in PA-1 and SKOV3 cells. Histone H3 and α-tubulin are loading controls.

(C–G) Immunofluorescence shows Peptidase M84 induced nuclear translocation of p50 (green) and p65 (green) in PA-1 and SKOV3 cells. Bar diagrams represent the ratio of the MFI of nucleus to cytosol of cells.

(H and I) Western blot with bar diagram of densitometric scan show significant upregulation in phospho-p38 and down-regulation in phospho-ERK-1/2 expression levels in Peptidase M84 treated PA-1 and SKOV3 cells. Here, GAPDH is used as loading control (J) Peptidase M84 mediated cellular apoptosis is analyzed by FACS in the presence and absence of different signaling inhibitors (PAR-1, NF-κB, p38, and ROS) and PAR-1 si-RNA in PA-1 (upper panel) and SKOV3 (lower panel) cells. (K and L) The above results are graphically represented in the bar diagram. In each panel, error bars were calculated based on results obtained from a minimum of three independent experiments. All statistical analysis was done by applying Student's t test (two-tailed). In all panels, ns $p > 0.05$, *$p \leq 0.05$, **$p \leq 0.01$, and ***$p \leq 0.001$. Data are expressed in ±SEM. Scale bars: 10 μm. Densitometric analysis was performed on ImageJ and Gel Quant softwares. Band intensities were normalized to loading controls. Fluorescence intensity and Pearson's co-efficient values were measured manually by drawing lines along the entire length of each nucleus or cytosol and calculating them using Fiji (https://imagej.net/software/fiji/). See also Figures S9–S11 and S13.

or creatinine and urea (parameters for toxin-induced impaired renal function) in the serum sample of experimental mice implicate hepatotoxicity and nephrotoxicity. ALT and AST activity was significantly upregulated and creatinine and urea levels were reduced significantly in the tumor control group when compared to the normal group. However, no such significant difference was noticed in all the aforementioned indexes in the only protease treated group with respect to normal untreated group. Our results deciphered that both liver and kidney toxicity parameters remained within the normal range after treatment with 3.0 μg/mL (12.0 μg/kg of body weight) of Peptidase M84 for up to 45 days of continual treatment (Figures 7J–7M). No adverse effects were observed concerning normal untreated mice. Upon evaluating the chronic toxicity of Peptidase M84, it did not cause any significant toxicity as all the parameters for liver and kidney toxicity lied within normal limit. We further validated those findings by histopathological analysis.

Peptidase M84 treatment showed recovery of the damaged architecture of liver and kidney tissue of host system and did not cause any significant toxicity

In the current investigation, histopathological examination was executed on sections from kidney and liver tissues of all six groups of experimental animals after 45 days of treatment using hematoxylin-eosin staining to assess whether there was any inconsistency with the biochemical markers. Histopathological sections of normal liver unraveled healthy morphology of hepatocytes; normal kidney tissues displayed healthy glomeruli, vessels, and tubules. However, tumor control group (group-2) showed disrupted architecture with moderate to dense inflammation with damaged hepatocytes in the liver and extensively damaged glomerular structure in the kidney. After Peptidase M84 treatment (group-3) this damage was observed to be recovered and healthy tissue structure prevailed in the liver and kidney tissue. In comparison with the untreated control group, no noticeable anomalies in the histopathology of the kidney and liver of the Peptidase M84 treated group-3 and group-4 were detected, following 45 days of continual treatment. Morphology of the liver of only Peptidase M84 treated mice was almost similar to the untreated group. Morphology of the livers from group-6 showed no significant change from that of the untreated control. As observed in untreated control, in addition to the radial distribution pattern of hepatocytes encircling the central vein was obvious in the protease control and vehicle control group after treatment. Radially arranged hepatocytes (HCs) lacking Kupffer cells (KCs) and fine integrity in the liver tissue, depict the absence of any chronic toxicity (Figure 7N).

Notable differences after 45 days of constant treatment with Peptidase M84 between renal corpuscles (RCs) and glomerular tufts of kidney tissue were not found when compared to the untreated group. Moreover, paucity of tubular dilation, glomerular infiltration, and necrosis indicated the non-existence of acute inflammation (Figure 7O). Hence, this implies that 3.0 μg/mL (12.0 μg/kg of body weight) of Peptidase M84 for the mentioned period is significantly non-toxic, non-hazardous to normal tissue of mice and does not affect the survival of mice (Figures 7N and 7O).

DISCUSSION

Emerging complexities and side effects associated with conventional chemotherapy necessitate the quest for new therapeutic agents for ovarian cancer treatment. In this study, we designed a novel approach to isolate and characterize proteases of environmental microbial origin for apoptotic properties to curb the growth of ovarian cancer cells. For this purpose, we assessed over 200 environmental isolates to finally select a protease secreting strain "GDL-186" which was identified as *Bacillus altitudinis*. Reported to be first isolated from air samples of high altitudes in India, *Bacillus altitudinis* was found to secrete extracellular proteases potentiating apoptosis in ovarian cancer cells in our study.[50] Popularly, *Bacillus* spp. is widely studied for its extracellular alkaline protease secreting properties which also make it industrially important.[51] In our attempt to find a protease with pro-apoptotic properties, we identified Peptidase M84 which is a key secretory metallo-protease of *Bacillus altitudinis*.[52] A recent report revealed the anti-proliferative activity of the organic extract of *Bacillus altitudinis* MTCC13046 against human hepatocellular carcinoma cells.[53] We obtained two major bands at 25 kDa and 16 kDa in SDS-PAGE for this purified protease which was homologous to the amino acid sequences of Peptidase M84 from *Bacillus altitudinis* in Uniprot (ID: A0A5D4PNG4) and NCBI databases. This protease is comprised of a conserved metallo-protease domain with three histidine residues in its active site, which is also reported to be present in metzincin metallo-protease from *Bacillus intermedius*.[39] The optimal protease activity of Peptidase M84 was observed in normal physiological pH (7.0–9.0) and temperature (37°C–40°C) that got inhibited by EDTA and 1,10 phenanthroline. This aided us to characterize

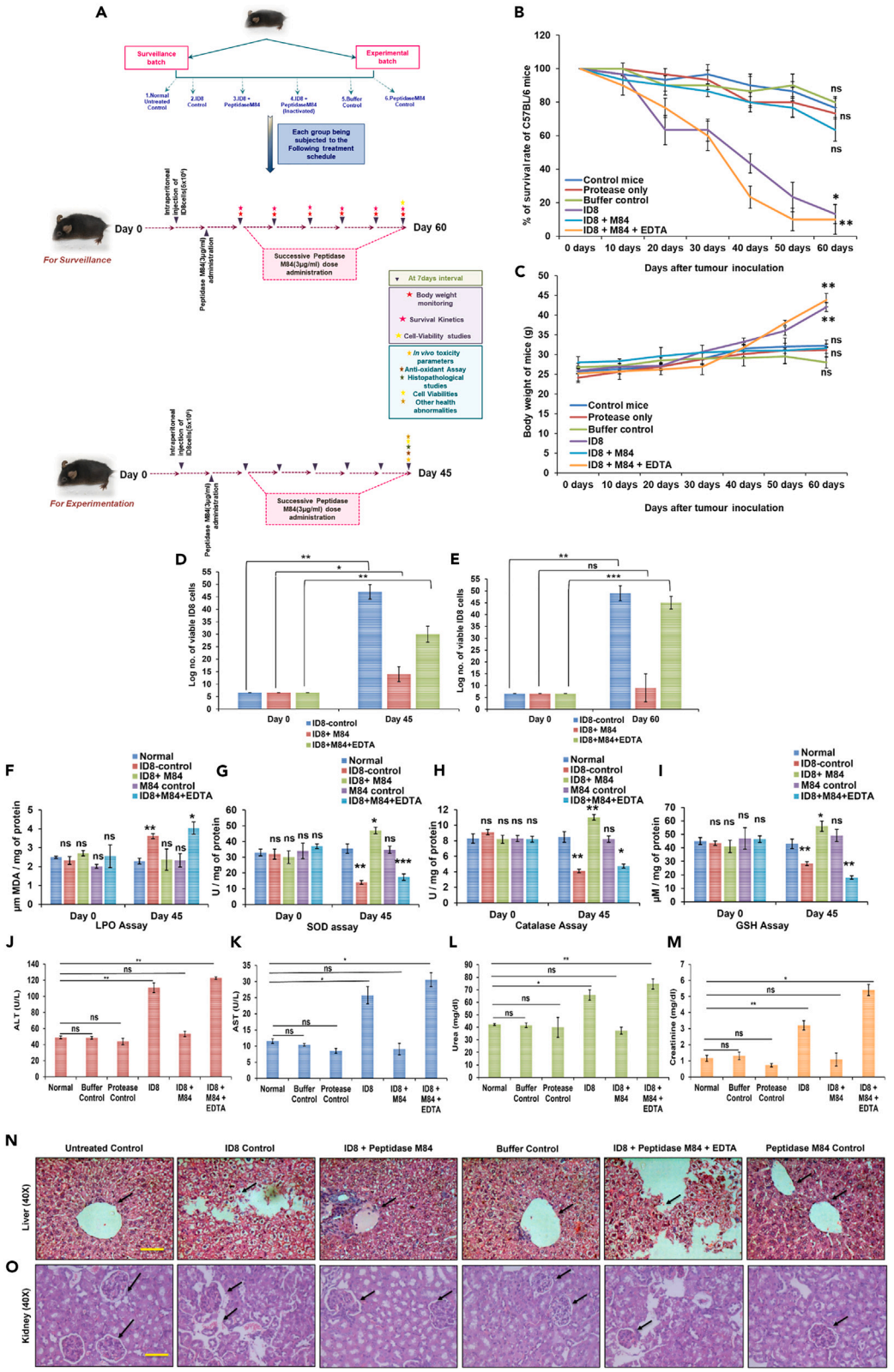
A
Surveillance batch
Experimental batch
1.Normal Untreated Control
2.ID8 Control
3.ID8 + PeptidaseM84
4.ID8 + PeptidaseM84 (Inactivated)
5.Buffer Control
6.PeptidaseM84 Control
Each group being subjected to the Following treatment schedule
Intraperitoneal injection of ID8cells(5x10⁶)
Day 0
Day 60
For Surveillance
Peptidase M84(3µg/ml) administration
Successive Peptidase M84(3µg/ml) dose administration
At 7days interval
Body weight monitoring
Survival Kinetics
Cell-Viability studies
In vivo toxicity parameters
Anti-oxidant Assay
Histopathological studies
Cell Viabilities
Other health abnormalities
Day 45
For Experimentation
B
% of survival rate of C57BL/6 mice
Control mice
Protease only
Buffer control
ID8
ID8 + M84
ID8 + M84 + EDTA
0 days 10 days 20 days 30 days 40 days 50 days 60 days
Days after tumour inoculation
C
Body weight of mice (g)
Days after tumour inoculation
D
Log no. of viable ID8 cells
Day 0
Day 45
ID8-control
ID8+ M84
ID8+M84+EDTA
E
Log no. of viable ID8 cells
Day 0
Day 60
F
µm MDA / mg of protein
LPO Assay
G
U / mg of protein
SOD assay
H
U / mg of protein
Catalase Assay
I
µM / mg of protein
GSH Assay
Normal
ID8-control
ID8+ M84
M84 control
ID8+M84+EDTA
J
A.L.T (U/L)
K
A.S.T (U/L)
L
Urea (mg/dl)
M
Creatinine (mg/dl)
Normal
Buffer Control
Protease Control
ID8
ID8 + M84
ID8 + M84 + EDTA
N
Untreated Control
ID8 Control
ID8 + Peptidase M84
Buffer Control
ID8 + Peptidase M84 + EDTA
Peptidase M84 Control
Liver (40X)
O
Kidney (40X)

Figure 7. Effect of Peptidase M84 on histological, biochemical parameters, survival rate, and body weight of tumor induced mice

(A) Illustration of the *in vivo* study to determine the anticancer potential and non-toxicity of Peptidase M84.

(B) Peptidase M84 treatment shows promising improvement in survival rate in ID8 mice model. Peptidase M84 in the presence of EDTA shows a similar mortality rate as tumor control group.

(C) Line graph shows body weight after Peptidase M84 administration in mice.

(D and E) Viable ID8 cells were measured at different time points by the trypan blue exclusion method.

(F–I) Biochemical parameters of cellular oxidative stress (LPO, SOD, CAT, and GSH) were measured in serum samples of mice. The results are graphically represented.

(J–M) Liver and kidney functionality test (ALT, AST, urea, and creatinine) was performed in serum samples of mice. The results are graphically represented.

(N and O) Histological studies (HandE staining) showed that Peptidase M84 treatment improved the damaged architecture of the liver and kidney tissue caused by tumor induction. While arrows indicated intact membrane integrity in control and Peptidase M84 treated set and disrupted tissue architectures in ID8 control and Peptidase M84-pre-treated with EDTA set. In each panel, error bars were calculated based on results obtained from a minimum of three independent experiments ($n = 3$). All statistical analysis was done by applying Student's t test (two-tailed). Data are expressed in $\pm$SEM. In all panels, ns $p > 0.05$, *$p \leq 0.05$, **$p \leq 0.01$, and ***$p \leq 0.001$. Scale bars: standard See also Figure S12.

Peptidase M84 as a Zn^{2+}-dependent metalloprotease. The LC-MS/MS peptide blast analysis showed the presence of Peptidase M84-like protease in other closely related Bacillus species such as *Bacillus aerophilus*, *Bacillus xiamenensis*, and *Bacillus intermedius*. However, the functional aspects especially the anticancer effects of these proteases were not elucidated well earlier. In this study, we report the apoptotic effects of this protease from an environmental isolate of *Bacillus altitudinis GDL-186* with high selective toxicity in ovarian cancer cells. Earlier studies majorly illustrated the biophysical and microbiological aspects of Peptidase M84. So, at present it is difficult to comment whether the previously identified Peptidase M84-like protease had any pro-apoptotic effect or not. Our work, in the present scenario, has definitely paved the way for further study in this direction in days to come. Previously, a polypeptide PBN118 isolated from a marine Bacillus was reported to be similar to the Peptidase M84 from *Bacillus pumilus*. PBN118 prevented migration and suppressed invasion of human hepatocellular carcinoma cells.[54]

Peptidase M84, here also triggered apoptosis in both human and mouse ovarian adenocarcinoma cells in a dose-dependent manner. Moreover, this pro-apoptotic response of Peptidase M84 was inhibited by EDTA treatment which helped us confirm that its apoptotic response was a result of its proteolytic activity. Interestingly, Peptidase M84 did not show any significant effect on IOSE and PEMΦ cells which were the normal cells used in this study. Additionally, Peptidase M84 turned out to be anti-proliferative in nature when it reduced the expression levels of Ki-67, a proliferative antigen in PA-1 and SKOV3 cells. Based on these findings, we were intrigued to decipher the detailed molecular mechanisms underlying the Peptidase M84 induced apoptosis in ovarian cancer cells. Since more than 90% of all ovarian malignancies are classified as EOC including the aggressive high-grade serous carcinoma category,[1] we considered that initial testing of Peptidase M84 for its apoptosis-inducing capabilities in *in vitro* setup could enable the designing of a better treatment rationale.

The canonical intrinsic pathway of apoptosis depends on the delicate balance between pro-apoptotic Bax and anti-apoptotic Bcl2.[55] We observed a significant increase in Bax to Bcl2 ratio, and a rise in cytosolic mitochondrial cytochrome *c* concentrations in addition to caspase 9 and 3 activation following Peptidase M84 treatment in SKOV3 as well as PA-1 cells. These observations delineated an induction of intrinsic apoptosis pathway in these malignant ovarian cells by Peptidase M84 specifically. Enhanced oxidative stress owing to the production of higher ROS and impaired redox balance is intrinsic to the sustenance of any neoplastic cells unlike a normal healthy cell.[25,26] In coherence with this fact, we also noted that Peptidase M84 abnormally increased intracellular ROS levels in PA1, SKOV3, and ID8 cells in a time-dependent manner which resulted in their apoptotic death. Contrastingly, Peptidase M84 failed to impart any such change in normal IOSE cells where ROS was quantitated to be very less with respect to the *in vitro* malignant setups. This observation was further confirmed by the inhibition of ROS by pre-incubation with NAC (a cellular ROS quencher) before treatment with Peptidase M84 in ovarian cancer cells. Overproduction and accumulation of ROS are known to modify nucleotides, break DNA strands, and facilitate chromosomal rearrangements, contributing to the deregulation of a wide range of signaling pathways.[56] Peptidase M84 treatment induced ROS-mediated DNA damage in ovarian cancer cells which intrigued us to check the status of mitochondrial membrane potential by JC-1 staining as ROS overproduction is always positively associated with mitochondrial membrane depolarization and reduced cell viability. A disruption in mitochondrial membrane potential by increased cellular ROS was apparent in JC1-stained ovarian cancer cells. These findings aligned with a rise of cytochrome *c* as detected in the cytosolic fractions of Peptidase M84 treated ovarian cancer cells which might have leaked out of a depolarized mitochondrial membrane to trigger apoptosis cascades involving caspases, apoptosome complex, and PARP.[46,57] Enzymatic activity of PARP is found to be increased in the cells under stressed conditions. Intact PARP expression is associated with DNA repair system which in turn saves the cancer cells from apoptotic cell death. The presence of cleaved PARP and a decrease in Bcl-2 muddle the apoptotic balance and drive the cell toward the gateway of apoptosis, as it restricts cell repair.[58] We evidenced Peptidase M84 to induce PARP cleavage in ovarian cancer cells which corroborated with an increased DNA damage. This PARP activating feature of Peptidase M84 is promising enough since the FDA has approved Olaparib (AZD2281) which is a PARP inhibitor for conventional ovarian cancer treatment.[59]

The major signaling pathways of proteases are initiated by the cleavage of PARs which play an important role both in cancer progression and apoptosis of malignant cells in a cue-based manner.[28] PAR-1 was reported to be overexpressed in explants of human ovarian cancer tissues compared to normal ovarian cells.[29,34] Gingipain-R (RgpB) a cysteine protease isolated from *Porphyromonas gingivalis* was the earliest reported microbial protease that acted by cleaving a model peptide representing a cleavage site of PAR-2.[60] We noted an overexpression of PAR-1 at both transcriptional and translational levels in Peptidase M84 treated ovarian cancer cells compared to their untreated counterparts. Interestingly, no significant alteration in the expression level of PAR-1 in Peptidase M84 treated normal ovarian epithelial cells was seen. Several evidence identified PAR-1 as a tumor promoter as it was associated with the induction of angiogenesis, invasion, and also metastasis

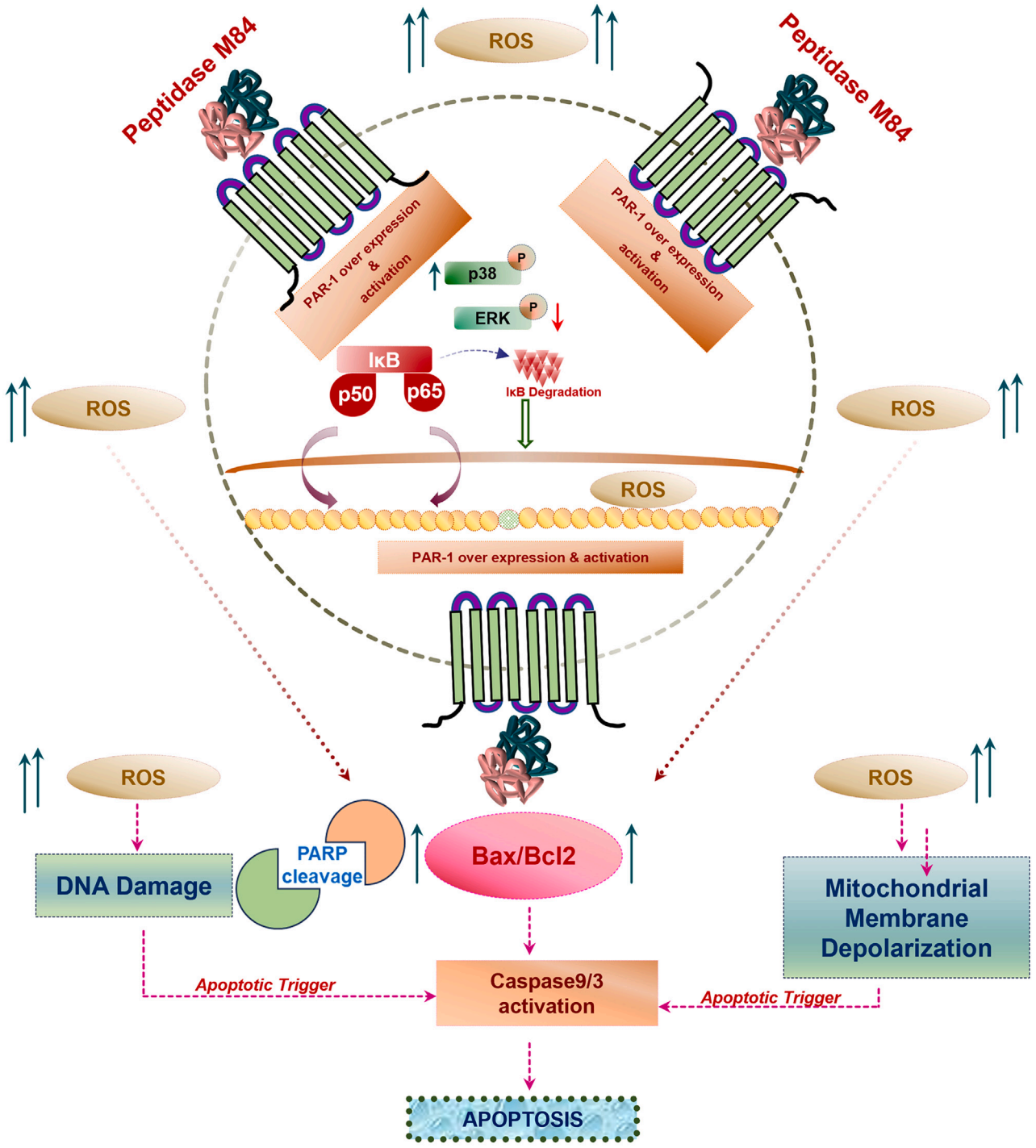

Figure 8. Schematic representation of Peptidase M84 induced apoptosis in ovarian cancer cells

Peptidase M84 induced activation and overexpression of PAR-1 thus enhancing cellular ROS and activation of NF-κB, p38 followed by downregulation of pERK1/2. ROS mediated DNA damage induced changes in mitochondrial membrane potential and triggered the release of mitochondrial cytochrome *c* which subsequently activated caspase 3 ultimately promoting Bax, Bcl2 mediated intrinsic pathway of apoptosis. Enhanced ROS level in malignant cells allows to meet the threshold level of cellular ROS that affect cell survival earlier than the normal healthy cells ultimately triggering apoptotic cell death.

in ovarian and breast adenocarcinoma cells along with xenograft models.[61,62] However, thrombin is found to mediate apoptosis in a dose-dependent way through modulation of PAR-1 in tumor cells.[33] Previously we reported that metallo-protease HAP from *V. cholerae* could cause overexpression of PAR-1 by inducing its cleavage.[37] Nevertheless, such a paradox is not limited only to PAR-1. Biomolecules like granulocyte/macrophage colony-stimulating factor, RAR-β2, E-cadherin, CD44, α/β-catenin, and CAV1 have also been reported to impart such contrasting functions in tumorigenesis.[41,63] In order to reveal the relationship between alteration in PAR-1 expression and apoptosis in the presence of Peptidase M84 in ovarian cancer cells, we performed gene knockdown, signaling inhibition, and immunoprecipitation studies. Our findings also demonstrated that Peptidase M84 could specifically bind and interact with PAR-1. Moreover, Peptidase M84 failed to induce apoptosis in PAR-1 silenced ovarian cancer cells. Furthermore, ML161, a PAR1-mediated Gq signaling inhibitor[64] also showed a significant decrease in apoptosis in Peptidase M84 treated cells. This suggests that Peptidase M84 caused PAR-1 activation through Gq signaling induction. Cumulative data strengthened the possible correlation regarding the role of PAR-1 in induction of apoptosis and established PAR-1 as a novel oncogenic target for Peptidase M84 mediated apoptosis in ovarian cancer cells. PAR1 has emerged as a promising hot spot target for chemotherapeutic drugs in recent years as well. PAR1 targeting drugs like vorapaxar and atropaxar have entered phases of clinical trials.[31]

Thrombin-mediated PAR-1 activation regulates major signaling pathways, such as p38 MAPK[47] and NF-κB.[48] Herein, inhibition studies using NF-κB and p38 inhibitors confirmed the involvement of NF-κB and MAPK in Peptidase M84-mediated apoptosis in PA-1 and SKOV3 cells. Pre-treatment with NF-κB, p38, and ROS inhibitors downregulated cellular apoptosis even after Peptidase M84 treatment compared to the absence of any prior inhibition. Interestingly, besides the upregulation of p38 phosphorylation, we also observed downregulation of *p*-ERK1/2 in these cells upon Peptidase M84 treatment. Blockade of AKT/ERK pathway and enhanced phosphorylation levels of p38, contributing majorly to apoptosis in response to different stimuli in cancer cells.[65] Furthermore, NF-κB regulates gene expression in cellular processes like cellular proliferation, stress responses, and apoptosis under different stimulations.[66] Besides, ROS can also regulate either activation or repression of NF-κB signaling depending on phase and context.[67,68] We noticed that the cellular ROS level was gradually increased with time by Peptidase M84 treatment in ovarian cancer cells. Peptidase M84 promoted PAR-1 dependent activation of p38 and NF-κB signaling which can augment the cellular ROS levels as well as inhibition of these signalings attenuated ROS levels in ovarian cancer cells. Phosphorylation of p38, a major component of MAPK pathway is linked with ROS generation and cell proliferation in the majority of the events.[49,69] However, when p-p38 levels cross the critical threshold in conjugation with the downregulation of ERK, cells get immensely stressed to meet death.[70] In addition, there was no significant expression of PAR-1 in IOSE cells. Therefore, the load of cellular ROS level was found to be lower in IOSE cells even after Peptidase M84 treatment as compared to cancer cells, as there was no effective alteration in PAR-1 activity or expression. Thus, Peptidase M84 failed to trigger the intrinsic apoptotic pathway in normal IOSE cells. In light of these findings, we established that PAR-1, NF-κB, p38, ERK1/2, and ROS regulate Peptidase M84-induced apoptosis by playing decisive roles in a collaborative manner in ovarian cancer cells (Figure 8).

Finally, to validate our findings *in vivo* we investigated the role of Peptidase M84 in a syngeneic mouse model. ID8 is a spontaneous murine ovarian adenocarcinoma cell line used to study ovarian tumor biology. This cell line is advantageous due to its efficacy in developing tumors in both solid and ascitic forms.[71,72] Herein, we report that Peptidase M84 treatment in ID8-mice resulted in inhibition of body weight increase due to less ascites formation. An increase in the survival rate of the ID8-bearing mice following Peptidase M84 treatment as compared to the tumor control group indicated that Peptidase M84 treatment affected the viability of cancer cells *in vivo*. However, Peptidase M84 pre-treated with EDTA was found to be ineffectual and did not show any kind of alterations. This indicated the antitumour activity of Peptidase M84 was linked to its proteolytic activity. In the ID8-bearing mice, the cellular ROS level was increased significantly after Peptidase M84 treatment. An increase in the Peptidase M84 induced oxidative stress corroborated with a rise in the levels of GSH, SOD, and catalase along with reduced LPO titers in the ID8-bearing mice receiving Peptidase M84 treatment as compared to the ID8 control mice. Moreover, the reduction in viable ID8 cell count in mouse peritoneum indicated that Peptidase M84 treatment decreased the survivability of tumor cells and strengthened the remedial effect of chemotherapy. The histopathological studies illustrated that the cellular architecture and morphology of the liver and kidney tissues of mice were not affected by Peptidase M84. Hence, it is significantly non-toxic for normal tissue of mice. However, Peptidase M84 treatment was capable of recovering the damaged tissue morphology in ID8-bearing mice. The increase in the levels of SGOT, SGPT, urea, and creatinine in the ID8 control group with respect to the Peptidase M84 treated group in regular intervals further validated our findings. No significant mortality or toxic symptoms were noticed in only Protease control group. Thus, our findings demonstrated a reduction in cancer cell proliferation via oxidative stress-mediated apoptosis without causing harm to normal healthy cells following Peptidase M84 treatment *in vivo*.

Limitations of the study

Unlike thrombin, the Peptidase M84 mediated exact PAR-1 cleavage site is in the process of identification which will be the major focus of our future study. Further investigations may be executed in other experimental models and clinical settings to enlist Peptidase M84 as an anti-cancer drug, which may widen the amplitude for a long-lasting targeted therapy for ovarian cancer. Thus, Peptidase M84 warrants further exploration as a new antitumour agent.

STAR★METHODS

Detailed methods are provided in the online version of this paper and include the following:

- KEY RESOURCES TABLE
- RESOURCE AVAILABILITY

SUPPLEMENTAL INFORMATION

Supplemental information can be found online at https://doi.org/10.1016/j.isci.2024.109828.

ACKNOWLEDGMENTS

This work was supported by the Indian Council of Medical Research adhoc project grant BMS/adhoc/56/2020-21 dt: 23.01.2021. Mr. Niraj Nag is thankful to the University Grants Commission, India for providing fellowship under the prestigious UGC-NET-JRF fellowship award (UGC-ref. no.: 757/CSIR-UGC-NET JUNE 2017).

We wish to express our gratefulness to Dr. Shanta Dutta (Director, ICMR-NICED) for providing us with the central research instrumentation facility of NICED. Mr. Biplab Roy (NICED) is acknowledged for helping us in the screening of environmental isolates. We sincerely thank Dr. Sib Sankar Roy (CSIR-IICB) for providing us with cell lines and Dr. Shruti Chatterjee (Nirma University) for providing us with all the bacterial isolates. We thankfully acknowledge Ms. Ritoja Shee (Manipal University Jaipur), Dr. Mainak Chakraborty (NICED), Mr. Prolay Halder (NICED), Ms. Suparna Chakraborty (NICED), Dr. Sutapa Mukherjee (CNCI), Mr. Arup Dutta Roy (Association of Chartered Certified Accountants, UK), and Dr. Atish Barua (Tufts University, USA) for their technical support and co-operation during the study.

AUTHOR CONTRIBUTIONS

N.N. conceptualized the study, investigated, performed experiments, wrote the original draft, reviewed, data curation, and analyzed and validated the data; T.R. performed experiments and reviewed; R.T. formal analysis and reviewed; A.G. performed experiments; R.D. formal

analysis of confocal imaging data; E.M. formal analysis and reviewed; S.S. formal analysis; A.P. flowcytometric data acquisition and formal analysis; P.P. provided resources; A.P. conceptualized the study, supervised the research work, funding acquisition, data curation, reviewed and approved the final manuscript.

Consent to publish: Not applicable.

DECLARATION OF INTERESTS

The authors declare no competing interests.

Received: October 5, 2023
Revised: January 2, 2024
Accepted: April 24, 2024
Published: April 26, 2024

REFERENCES

1. Ciucci, A., Buttarelli, M., Fagotti, A., Scambia, G., and Gallo, D. (2022). Preclinical models of epithelial ovarian cancer: practical considerations and challenges for a meaningful application. Cell. Mol. Life Sci. *79*, 364. https://doi.org/10.1007/s00018-022-04395-y.
2. Kurnit, K.C., Fleming, G.F., and Lengyel, E. (2021). Updates and New Options in Advanced Epithelial Ovarian Cancer Treatment. Obstet. Gynecol. *137*, 108–121. https://doi.org/10.1097/AOG.0000000000004173.
3. Moschetta, M., Boussios, S., Rassy, E., Samartzis, E.P., Funingana, G., and Uccello, M. (2020). Neoadjuvant treatment for newly diagnosed advanced ovarian cancer: where do we stand and where are we going? Ann. Transl. Med. *8*, 1710. https://doi.org/10.21037/atm-20-1683.
4. Huang, M., Lu, J.J., and Ding, J. (2021). Natural Products in Cancer Therapy: Past, Present and Future. Nat. Prod. Bioprospect. *11*, 5–13. https://doi.org/10.1007/s13659-020-00293-7.
5. Barua, A., Choudhury, P., Nag, N., Nath, A., Kundagrami, S., Pal, A., Panda, C.K., and Saha, P. (2022). Xanthone from Swertia chirata exerts chemotherapeutic potential against colon carcinoma. Curr. Sci. *122*, 47–55.
6. Mehta, J., Rayalam, S., and Wang, X. (2018). Cytoprotective Effects of Natural Compounds against Oxidative Stress. Antioxidants *7*, 147. https://doi.org/10.3390/antiox7100147.
7. Sahayasheela, V.J., Lankadasari, M.B., Dan, V.M., Dastager, S.G., Pandian, G.N., and Sugiyama, H. (2022). Artificial intelligence in microbial natural product drug discovery: current and emerging role. Nat. Prod. Rep. *39*, 2215–2230. https://doi.org/10.1039/d2np00035k.
8. Li, P., Li, X., Saravanan, R., Li, C.M., and Leong, S.S.J. (2012). Antimicrobial macromolecules: synthesis methods and future applications. RSC Adv. *2*, 4031–4044.
9. Ab Mutalib, N.S., Wong, S.H., Ser, H.L., Duangjai, A., Law, J.W.F., Ratnakomala, S., Tan, L.T.H., and Letchumanan, V. (2020). Bioprospecting of microbes for valuable compounds to mankind. Prog. Micobes. Mol. Biol. *3*.
10. Carswell, E.A., Old, L.J., Kassel, R.L., Green, S., Fiore, N., and Williamson, B. (1975). An endotoxin-induced serum factor that causes necrosis of tumors. Proc. Natl. Acad. Sci. USA *72*, 3666–3670. https://doi.org/10.1073/pnas.72.9.3666.
11. Trivanović, D., Pavelić, K., and Peršurić, Ž. (2021). Fighting Cancer with Bacteria and Their Toxins. Int. J. Mol. Sci. *22*, 12980. https://doi.org/10.3390/ijms222312980.
12. Xu, Y., Kersten, R.D., Nam, S.J., Lu, L., Al-Suwailem, A.M., Zheng, H., Fenical, W., Dorrestein, P.C., Moore, B.S., and Qian, P.Y. (2012). Bacterial biosynthesis and maturation of the didemnin anti-cancer agents. J. Am. Chem. Soc. *134*, 8625–8632. https://doi.org/10.1021/ja301735a.
13. Punj, V., Bhattacharyya, S., Saint-Dic, D., Vasu, C., Cunningham, E.A., Graves, J., Yamada, T., Constantinou, A.I., Christov, K., White, B., et al. (2004). Bacterial cupredoxin azurin as an inducer of apoptosis and regression in human breast cancer. Oncogene *23*, 2367–2378. https://doi.org/10.1038/sj.onc.1207376.
14. Nadeem, A., Aung, K.M., Ray, T., Alam, A., Persson, K., Pal, A., Uhlin, B.E., and Wai, S.N. (2021). Suppression of β-catenin signaling in colon carcinoma cells by a bacterial protein. Int. J. Cancer *149*, 442–459. https://doi.org/10.1002/ijc.33562.
15. Toh, E., Baryalai, P., Nadeem, A., Aung, K.M., Chen, S., Persson, K., Persson, J.L., Uhlin, B.E., and Wai, S.N. (2022). Bacterial protein MakA causes suppression of tumour cell proliferation via inhibition of PIP5K1α/Akt signalling. Cell Death Dis. *13*, 1024. https://doi.org/10.1038/s41419-022-05480-7.
16. Taggart, C.C., Greene, C.M., Smith, S.G., Levine, R.L., McCray, P.B., Jr., O'Neill, S., and McElvaney, N.G. (2003). Inactivation of human beta-defensins 2 and 3 by elastolytic cathepsins. J. Immunol. *171*, 931–937. https://doi.org/10.4049/jimmunol.171.2.931.
17. Moncada, D., Keller, K., and Chadee, K. (2003). Entamoeba histolytica cysteine proteinases disrupt the polymeric structure of colonic mucin and alter its protective function. Infect. Immun. *71*, 838–844. https://doi.org/10.1128/IAI.71.2.838-844.2003.
18. Denecker, G., Declercq, W., Geuijen, C.A., Boland, A., Benabdillah, R., van Gurp, M., Sory, M.P., Vandenabeele, P., and Cornelis, G.R. (2001). Yersinia enterocolitica YopP-induced apoptosis of macrophages involves the apoptotic signaling cascade upstream of bid. J. Biol. Chem. *276*, 19706–19714. https://doi.org/10.1074/jbc.M101573200.
19. Maeda, H., Matsumura, Y., and Molla, A. (1987). Antitumor activity of some bacterial proteases: eradication of solid tumors in mice by intratumor injection. Cancer Res. *47*, 563–566.
20. Maeda, H., Molla, A., Sakamoto, K., Murakami, A., and Matsumura, Y. (1989). Cytotoxicity of bacterial proteases in various tumor cells mediated through alpha 2-macroglobulin receptor. Cancer Res. *49*, 660–664.
21. Singh, N., Tapader, R., Chatterjee, S., Pal, A., and Pal, A. (2022). Subtilisin from Bacillus amyloliquefaciens induces apoptosis in breast cancer cells through ubiquitin-proteasome-mediated tubulin degradation. Int. J. Biol. Macromol. *220*, 852–865. https://doi.org/10.1016/j.ijbiomac.2022.08.086.
22. Pieters, R., Hunger, S.P., Boos, J., Rizzari, C., Silverman, L., Baruchel, A., Goekbuget, N., Schrappe, M., and Pui, C.H. (2011). L-asparaginase treatment in acute lymphoblastic leukemia: a focus on Erwinia asparaginase. Cancer *117*, 238–249. https://doi.org/10.1002/cncr.25489.
23. Alrumman, S.A., Mostafa, Y.S., Al-Izran, K.A., Alfaifi, M.Y., Taha, T.H., and Elbehairi, S.E. (2019). Production and Anticancer Activity of an L-Asparaginase from Bacillus licheniformis Isolated from the Red Sea, Saudi Arabia. Sci. Rep. *9*, 3756. https://doi.org/10.1038/s41598-019-40512-x.
24. Pereira, F.V., Ferreira-Guimarães, C.A., Paschoalin, T., Scutti, J.A.B., Melo, F.M., Silva, L.S., Melo, A.C.L., Silva, P., Tiago, M., Matsuo, A.L., et al. (2014). A natural bacterial-derived product, the metalloprotease arazyme, inhibits metastatic murine melanoma by inducing MMP-8 cross-reactive antibodies. PLoS One *9*, e96141. https://doi.org/10.1371/journal.pone.0096141.
25. Hayes, J.D., Dinkova-Kostova, A.T., and Tew, K.D. (2020). Oxidative Stress in Cancer. Cancer Cell *38*, 167–197. https://doi.org/10.1016/j.ccell.2020.06.001.
26. Perillo, B., Di Donato, M., Pezone, A., Di Zazzo, E., Giovannelli, P., Galasso, G., Castoria, G., and Migliaccio, A. (2020). ROS in cancer therapy: the bright side of the moon. Exp. Mol. Med. *52*, 192–203. https://doi.org/10.1038/s12276-020-0384-2.
27. Ray, T., Chakrabarti, M.K., and Pal, A. (2016). Hemagglutinin protease secreted by V. cholerae induced apoptosis in breast cancer cells by ROS mediated intrinsic pathway and regresses tumor growth in mice model. Apoptosis *21*, 143–154. https://doi.org/10.1007/s10495-015-1194-1.
28. Soh, U.J.K., Dores, M.R., Chen, B., and Trejo, J. (2010). Signal transduction by protease-activated receptors. Br. J. Pharmacol. *160*, 191–203. https://doi.org/10.1111/j.1476-5381.2010.00705.x.
29. Flynn, A.N., and Buret, A.G. (2004). Proteinase-activated receptor 1 (PAR-1) and

cell apoptosis. Apoptosis *9*, 729–737. https://doi.org/10.1023/B:APPT.0000045784.49886.96.

30. Sébert, M., Sola-Tapias, N., Mas, E., Barreau, F., and Ferrand, A. (2019). Protease-Activated Receptors in the Intestine: Focus on Inflammation and Cancer. Front. Endocrinol. *10*, 717. https://doi.org/10.3389/fendo.2019.00717.
31. Liu, X., Yu, J., Song, S., Yue, X., and Li, Q. (2017). Protease-activated receptor-1 (PAR-1): a promising molecular target for cancer. Oncotarget *8*, 107334–107345. https://doi.org/10.18632/oncotarget.21015.
32. Turk, B., Turk, D., and Turk, V. (2012). Protease signalling: the cutting edge. EMBO J. *31*, 1630–1643. https://doi.org/10.1038/emboj.2012.42.
33. Zain, J., Huang, Y.Q., Feng, X., Nierodzik, M.L., Li, J.J., and Karpatkin, S. (2000). Concentration-dependent dual effect of thrombin on impaired growth/apoptosis or mitogenesis in tumor cells. Blood *95*, 3133–3138.
34. Grisaru-Granovsky, S., Salah, Z., Maoz, M., Pruss, D., Beller, U., and Bar-Shavit, R. (2005). Differential expression of protease activated receptor 1 (Par1) and pY397FAK in benign and malignant human ovarian tissue samples. Int. J. Cancer *113*, 372–378. https://doi.org/10.1002/ijc.20607.
35. Chin, A.C., Vergnolle, N., MacNaughton, W.K., Wallace, J.L., Hollenberg, M.D., and Buret, A.G. (2003). Proteinase-activated receptor 1 activation induces epithelial apoptosis and increases intestinal permeability. Proc. Natl. Acad. Sci. USA *100*, 11104–11109. https://doi.org/10.1073/pnas.1831452100.
36. Mußbach, F., Henklein, P., Westermann, M., Settmacher, U., Böhmer, F.D., and Kaufmann, R. (2015). Proteinase-activated receptor 1- and 4-promoted migration of Hep3B hepatocellular carcinoma cells depends on ROS formation and RTK transactivation. J. Cancer Res. Clin. Oncol. *141*, 813–825. https://doi.org/10.1007/s00432-014-1863-4.
37. Ray, T., and Pal, A. (2016). PAR-1 mediated apoptosis of breast cancer cells by V. cholerae hemagglutinin protease. Apoptosis *21*, 609–620. https://doi.org/10.1007/s10495-016-1229-2.
38. Sheng, Y.N., Luo, Y.H., Liu, S.B., Xu, W.T., Zhang, Y., Zhang, T., Xue, H., Zuo, W.B., Li, Y.N., Wang, C.Y., and Jin, C.H. (2020). Zeaxanthin Induces Apoptosis via ROS-Regulated MAPK and AKT Signaling Pathway in Human Gastric Cancer Cells. OncoTargets Ther. *13*, 10995–11006. https://doi.org/10.2147/OTT.S272514.
39. Sabirova, A.R., Rudakova, N.L., Balaban, N.P., Ilyinskaya, O.N., Demidyuk, I.V., Kostrov, S.V., Rudenskaya, G.N., and Sharipova, M.R. (2010). A novel secreted metzincin metalloproteinase from Bacillus intermedius. FEBS Lett. *584*, 4419–4425. https://doi.org/10.1016/j.febslet.2010.09.049.
40. Gomes, M.S.R., Naves de Souza, D.L., Guimarães, D.O., Lopes, D.S., Mamede, C.C.N., Gimenes, S.N.C., Achê, D.C., Rodrigues, R.S., Yoneyama, K.A.G., Borges, M.H., et al. (2015). Biochemical and functional characterization of Bothropoidin: the first haemorrhagic metalloproteinase from Bothrops pauloensis snake venom. J. Biochem. *157*, 137–149. https://doi.org/10.1093/jb/mvu058.
41. Scholzen, T., and Gerdes, J. (2000). The Ki-67 protein: from the known and the unknown. J. Cell. Physiol. *182*, 311–322. https://doi.org/10.1002/(SICI)1097-4652(200003)182:3<311::AID-JCP1>3.0.CO;2-9.
42. Deb, M., Sengupta, D., Kar, S., Rath, S.K., Parbin, S., Shilpi, A., Roy, S., Das, G., and Patra, S.K. (2014). Elucidation of caveolin 1 both as a tumor suppressor and metastasis promoter in light of epigenetic modulators. Tumour Biol. *35*, 12031–12047. https://doi.org/10.1007/s13277-014-2502-z.
43. Higuchi, M., Honda, T., Proske, R.J., and Yeh, E.T. (1998). Regulation of reactive oxygen species-induced apoptosis and necrosis by caspase 3-like proteases. Oncogene *17*, 2753–2760. https://doi.org/10.1038/sj.onc.1202211.
44. von Harsdorf, R., Li, P.F., and Dietz, R. (1999). Signaling pathways in reactive oxygen species-induced cardiomyocyte apoptosis. Circulation *99*, 2934–2941. https://doi.org/10.1161/01.cir.99.22.2934.
45. Susin, S.A., Zamzami, N., Castedo, M., Daugas, E., Wang, H.G., Geley, S., Fassy, F., Reed, J.C., and Kroemer, G. (1997). The central executioner of apoptosis: multiple connections between protease activation and mitochondria in Fas/APO-1/CD95- and ceramide-induced apoptosis. J. Exp. Med. *186*, 25–37. https://doi.org/10.1084/jem.186.1.25.
46. Bossy-Wetzel, E., Newmeyer, D.D., and Green, D.R. (1998). Mitochondrial cytochrome c release in apoptosis occurs upstream of DEVD-specific caspase activation and independently of mitochondrial transmembrane depolarization. EMBO J. *17*, 37–49. https://doi.org/10.1093/emboj/17.1.37.
47. Marin, V., Farnarier, C., Grès, S., Kaplanski, S., Su, M.S., Dinarello, C.A., and Kaplanski, G. (2001). The p38 mitogen-activated protein kinase pathway plays a critical role in thrombin-induced endothelial chemokine production and leukocyte recruitment. Blood *98*, 667–673. https://doi.org/10.1182/blood.v98.3.667.
48. Rahman, A., True, A.L., Anwar, K.N., Ye, R.D., Voyno-Yasenetskaya, T.A., and Malik, A.B. (2002). Galpha(q) and Gbetagamma regulate PAR-1 signaling of thrombin-induced NF-kappaB activation and ICAM-1 transcription in endothelial cells. Circ. Res. *91*, 398–405. https://doi.org/10.1161/01.res.0000033520.95242.a2.
49. Tapader, R., Bose, D., Dutta, P., Das, S., and Pal, A. (2018). SslE (YghJ), a Cell-Associated and Secreted Lipoprotein of Neonatal Septicemic Escherichia coli, Induces Toll-Like Receptor 2-Dependent Macrophage Activation and Proinflammation through NF-κB and MAP Kinase Signaling. Infect. Immun. *86*, e00399-18. https://doi.org/10.1128/IAI.00399-18.
50. Shivaji, S., Chaturvedi, P., Suresh, K., Reddy, G.S.N., Dutt, C.B.S., Wainwright, M., Narlikar, J.V., and Bhargava, P.M. (2006). Bacillus aerius sp. nov., Bacillus aerophilus sp. nov., Bacillus stratosphericus sp. nov. and Bacillus altitudinis sp. nov., isolated from cryogenic tubes used for collecting air samples from high altitudes. Int. J. Syst. Evol. Microbiol. *56*, 1465–1473. https://doi.org/10.1099/ijs.0.64029-0.
51. Rao, M.B., Tanksale, A.M., Ghatge, M.S., and Deshpande, V.V. (1998). Molecular and biotechnological aspects of microbial proteases. Microbiol. Mol. Biol. Rev. *62*, 597–635. https://doi.org/10.1128/MMBR.62.3.597-635.1998.
52. Nguyen, T.T.H., Myrold, D.D., and Mueller, R.S. (2019). Distributions of Extracellular Peptidases Across Prokaryotic Genomes Reflect Phylogeny and Habitat. Front. Microbiol. *10*, 413. https://doi.org/10.3389/fmicb.2019.00413.
53. Asharaf, S., and Chakraborty, K. (2022). Seaweed-associated heterotrophic Bacillus altitudinis MTCC13046: a promising marine bacterium for use against human hepatocellular adenocarcinoma. Arch. Microbiol. *205*, 10. https://doi.org/10.1007/s00203-022-03346-2.
54. Zheng, L., Zhu, X., Yang, K., Zhu, M., Farooqi, A.A., Kang, D., Sun, M., Xu, Y., Lin, X., Feng, Y., et al. (2021). PBN11-8, a Cytotoxic Polypeptide Purified from Marine Bacillus, Suppresses Invasion and Migration of Human Hepatocellular Carcinoma Cells by Targeting Focal Adhesion Kinase Pathways. Polymers *13*, 166. https://doi.org/10.3390/polym13010166.
55. Yang, J., Liu, X., Bhalla, K., Kim, C.N., Ibrado, A.M., Cai, J., Peng, T.I., Jones, D.P., and Wang, X. (1997). Prevention of apoptosis by Bcl-2: release of cytochrome c from mitochondria blocked. Science *275*, 1129–1132. https://doi.org/10.1126/science.275.5303.1129.
56. Srinivas, U.S., Tan, B.W.Q., Vellayappan, B.A., and Jeyasekharan, A.D. (2019). ROS and the DNA damage response in cancer. Redox Biol. *25*, 101084. https://doi.org/10.1016/j.redox.2018.101084.
57. Goldstein, J.C., Waterhouse, N.J., Juin, P., Evan, G.I., and Green, D.R. (2000). The coordinate release of cytochrome c during apoptosis is rapid, complete and kinetically invariant. Nat. Cell Biol. *2*, 156–162. https://doi.org/10.1038/35004029.
58. Rath, S.K., Deb, M., Sengupta, D., Kari, V., Kar, S., Parbin, S., Pradhan, N., and Patra, S.K. (2016). Silencing of ZRF1 impedes survival of estrogen receptor positive MCF-7 cells and potentiates the effect of curcumin. Tumour Biol. *37*, 12535–12546. https://doi.org/10.1007/s13277-016-5114-y.
59. Kim, G., Ison, G., McKee, A.E., Zhang, H., Tang, S., Gwise, T., Sridhara, R., Lee, E., Tzou, A., Philip, R., et al. (2015). FDA Approval Summary: Olaparib Monotherapy in Patients with Deleterious Germline BRCA-Mutated Advanced Ovarian Cancer Treated with Three or More Lines of Chemotherapy. Clin. Cancer Res. *21*, 4257–4261. https://doi.org/10.1158/1078-0432.CCR-15-0887.
60. Lourbakos, A., Chinni, C., Thompson, P., Potempa, J., Travis, J., Mackie, E.J., and Pike, R.N. (1998). Cleavage and activation of proteinase-activated receptor-2 on human neutrophils by gingipain-R from Porphyromonas gingivalis. FEBS Lett. *435*, 45–48. https://doi.org/10.1016/s0014-5793(98)01036-9.
61. Agarwal, A., Covic, L., Sevigny, L.M., Kaneider, N.C., Lazarides, K., Azabdaftari, G., Sharifi, S., and Kuliopulos, A. (2008). Targeting a metalloprotease-PAR1 signaling system with cell-penetrating pepducins inhibits angiogenesis, ascites, and progression of ovarian cancer. Mol. Cancer Ther. *7*, 2746–2757. https://doi.org/10.1158/1535-7163.MCT-08-0177.
62. Boire, A., Covic, L., Agarwal, A., Jacques, S., Sherifi, S., and Kuliopulos, A. (2005). PAR1 is a matrix metalloprotease-1 receptor that promotes invasion and tumorigenesis of breast cancer cells. Cell *120*, 303–313. https://doi.org/10.1016/j.cell.2004.12.018.

63. Patra, S.K. (2008). Dissecting lipid raft facilitated cell signaling pathways in cancer. Biochim. Biophys. Acta *1785*, 182–206. https://doi.org/10.1016/j.bbcan.2007.11.002.
64. Gandhi, D.M., Rosas, R., Jr., Greve, E., Kentala, K., D-R Diby, N., Snyder, V.A., Stephans, A., Yeung, T.H.W., Subramaniam, S., DiMilo, E., et al. (2019). The parmodulin NRD-21 is an allosteric inhibitor of PAR1 Gq signaling with improved anti-inflammatory activity and stability. Bioorg. Med. Chem. *27*, 3788–3796. https://doi.org/10.1016/j.bmc.2019.06.043.
65. Yang, C., Luo, J., Luo, X., Jia, W., Fang, Z., Yi, S., and Li, L. (2020). Morusin exerts anti-cancer activity in renal cell carcinoma by disturbing MAPK signaling pathways. Ann. Transl. Med. *8*, 327. https://doi.org/10.21037/atm.2020.02.107.
66. Oeckinghaus, A., and Ghosh, S. (2009). The NF-kappaB family of transcription factors and its regulation. Cold Spring Harb. Perspect. Biol. *1*, a000034. https://doi.org/10.1101/cshperspect.a000034.
67. Lingappan, K. (2018). NF-κB in Oxidative Stress. Curr. Opin. Toxicol. *7*, 81–86. https://doi.org/10.1016/j.cotox.2017.11.002.
68. Nakajima, S., and Kitamura, M. (2013). Bidirectional regulation of NF-κB by reactive oxygen species: a role of unfolded protein response. Free Radic. Biol. Med. *65*, 162–174. https://doi.org/10.1016/j.freeradbiomed.2013.06.020.
69. Kulisz, A., Chen, N., Chandel, N.S., Shao, Z., and Schumacker, P.T. (2002). Mitochondrial ROS initiate phosphorylation of p38 MAP kinase during hypoxia in cardiomyocytes. Am. J. Physiol. Lung Cell Mol. Physiol. *282*, L1324–L1329. https://doi.org/10.1152/ajplung.00326.2001.
70. Berra, E., Diaz-Meco, M.T., and Moscat, J. (1998). The activation of p38 and apoptosis by the inhibition of Erk is antagonized by the phosphoinositide 3-kinase/Akt pathway. J. Biol. Chem. *273*, 10792–10797. https://doi.org/10.1074/jbc.273.17.10792.
71. Roby, K.F., Taylor, C.C., Sweetwood, J.P., Cheng, Y., Pace, J.L., Tawfik, O., Persons, D.L., Smith, P.G., and Terranova, P.F. (2000). Development of a syngeneic mouse model for events related to ovarian cancer. Carcinogenesis *21*, 585–591. https://doi.org/10.1093/carcin/21.4.585.
72. Janát-Amsbury, M.M., Yockman, J.W., Anderson, M.L., Kieback, D.G., and Kim, S.W. (2006). Comparison of ID8 MOSE and VEGF-modified ID8 cell lines in an immunocompetent animal model for human ovarian cancer. Anticancer Res. *26*, 2785–2789.
73. Kruk, P.A., Maines-Bandiera, S.L., and Auersperg, N. (1990). A simplified method to culture human ovarian surface epithelium. Lab. Invest. *63*, 132–136.
74. Ghosh, D., Pakhira, S., Ghosh, D.D., Roychoudhury, S., and Roy, S.S. (2023). Ets1 facilitates EMT/invasion through Drp1-mediated mitochondrial fragmentation in ovarian cancer. iScience *26*, 107537. https://doi.org/10.1016/j.isci.2023.107537.
75. Syngkon, A., Elluri, S., Koley, H., Rompikuntal, P.K., Saha, D.R., Chakrabarti, M.K., Bhadra, R.K., Wai, S.N., and Pal, A. (2010). Studies on a novel serine protease of a ΔhapAΔprtV Vibrio cholerae O1 strain and its role in hemorrhagic response in the rabbit ileal loop model. PLoS One *5*, e13122. https://doi.org/10.1371/journal.pone.0013122.
76. Tapader, R., Bose, D., Basu, P., Mondal, M., Mondal, A., Chatterjee, N.S., Dutta, P., Basu, S., Bhadra, R.K., and Pal, A. (2016). Role in proinflammatory response of YghJ, a secreted metalloprotease from neonatal septicemic Escherichia coli. Int. J. Med. Microbiol. *306*, 554–565. https://doi.org/10.1016/j.ijmm.2016.06.003.
77. Mondal, A., Tapader, R., Chatterjee, N.S., Ghosh, A., Sinha, R., Koley, H., Saha, D.R., Chakrabarti, M.K., Wai, S.N., and Pal, A. (2016). Cytotoxic and Inflammatory Responses Induced by Outer Membrane Vesicle-Associated Biologically Active Proteases from Vibrio cholerae. Infect. Immun. *84*, 1478–1490. https://doi.org/10.1128/IAI.01365-15.
78. Kar, S., Sengupta, D., Deb, M., Shilpi, A., Parbin, S., Rath, S.K., Pradhan, N., Rakshit, M., and Patra, S.K. (2014). Expression profiling of DNA methylation-mediated epigenetic gene-silencing factors in breast cancer. Clin. Epigenet. *6*, 20. https://doi.org/10.1186/1868-7083-6-20.
79. Chakraborty, M., and Bhaumik, M. (2020). Prenatal arsenic exposure interferes in postnatal immunocompetence despite an absence of ongoing arsenic exposure. J. Immunotoxicol. *17*, 135–143. https://doi.org/10.1080/1547691X.2020.1767238.
80. Naskar, D., Maiti, G., Chakraborty, A., Roy, A., Chattopadhyay, D., and Sen, M. (2014). Wnt5a-Rac1-NF-κB homeostatic circuitry sustains innate immune functions in macrophages. J. Immunol. *192*, 4386–4397. https://doi.org/10.4049/jimmunol.1302817.
81. Prasad, P., Ghosh, S., and Roy, S.S. (2021). Glutamine deficiency promotes stemness and chemoresistance in tumor cells through DRP1-induced mitochondrial fragmentation. Cell. Mol. Life Sci. *78*, 4821–4845. https://doi.org/10.1007/s00018-021-03818-6.
82. Singh, N.P., McCoy, M.T., Tice, R.R., and Schneider, E.L. (1988). A simple technique for quantitation of low levels of DNA damage in individual cells. Exp. Cell Res. *175*, 184–191. https://doi.org/10.1016/0014-4827(88)90265-0.
83. Das, R., Kamal, I.M., Das, S., Chakrabarti, S., and Chakrabarti, O. (2022). MITOL-mediated DRP1 ubiquitylation and degradation promotes mitochondrial hyperfusion in a CMT2A-linked MFN2 mutant. J. Cell Sci. *135*, jcs257808. https://doi.org/10.1242/jcs.257808.
84. Dimauro, I., Pearson, T., Caporossi, D., and Jackson, M.J. (2012). A simple protocol for the subcellular fractionation of skeletal muscle cells and tissue. BMC Res. Notes *5*, 513. https://doi.org/10.1186/1756-0500-5-513.
85. Li, J., Cui, J., Li, Z., Fu, X., Li, J., Li, H., Wang, S., and Zhang, M. (2020). ORP8 induces apoptosis by releasing cytochrome c from mitochondria in non-small cell lung cancer. Oncol. Rep. *43*, 1516–1524. https://doi.org/10.3892/or.2020.7517.
86. Sun, L., Xie, P., Wada, J., Kashihara, N., Liu, F.Y., Zhao, Y., Kumar, D., Chugh, S.S., Danesh, F.R., and Kanwar, Y.S. (2008). Rap1b GTPase ameliorates glucose-induced mitochondrial dysfunction. J. Am. Soc. Nephrol. *19*, 2293–2301. https://doi.org/10.1681/ASN.2008030336.
87. Barua, A., Choudhury, P., Maity, J.K., Mandal, S.B., Mandal, S., and Saha, P. (2019). Chemotherapeutic potential of novel non-toxic nucleoside analogues on EAC ascitic tumour cells. Free Radic. Res. *53*, 57–67. https://doi.org/10.1080/10715762.2018.1551999.
88. Dasgupta, S., Kar, K., Barua, A., Ghosh, D., Kabi, B., Dewan, K., and Chandra, A. (2022). A significantly non-toxic novel Cobalt(III) Schiff base complex induces apoptosis via G2-M cell cycle arrest in human breast cancer cell line MCF-7. Life Sci. *308*, 120963. https://doi.org/10.1016/j.lfs.2022.120963.
89. Barua, A., Choudhury, P., Mandal, S., Panda, C.K., and Saha, P. (2020). Therapeutic potential of xanthones from Swertia chirata in breast cancer cells. Indian J. Med. Res. *152*, 285–295. https://doi.org/10.4103/ijmr.IJMR_1153_18.

STAR★METHODS

KEY RESOURCES TABLE

REAGENT or RESOURCE	SOURCE	IDENTIFIER
Antibodies		
Anti-cleaved PARP antibody	Cell Signaling Technology	Cat# 5625; RRID:AB_10699459
Anti Bax antibody	Cell Signaling Technology	Cat# 5023; RRID:AB_10557411
Anti Bcl-2 antibody	Cell Signaling Technology	Cat# 15071; RRID:AB_2744528
Anti-caspase 8 antibody	Cell Signaling Technology	Cat# 9746; RRID:AB_2275120
Anti-Cytochrome c antibody	Cell Signaling Technology	Cat# 11940; RRID:AB_2637071
Anti-Histone H3 antibody	Cell Signaling Technology	Cat# 14269; RRID:AB_2756816
Anti-α-Tubulin antibody	Cell Signaling Technology	Cat# 3873; RRID:AB_1904178
Anti GAPDH antibody	Cell Signaling Technology	Cat# 97166; RRID:AB_2756824
Anti-Ki-67 antibody	Cell Signaling Technology	Cat# 9449; RRID:AB_2797703
Anti-cleaved caspase 9 antibody	Cell Signaling Technology	Cat# 7237; RRID:AB_10895832
Anti-p65 antibody	Cell Signaling Technology	Cat# 4764; RRID:AB_823578
Anti-p38 antibody	Cell Signaling Technology	Cat# 8690; RRID:AB_10999090
Anti-PAR-1 antibody	Millipore, Merck	Cat# MABF244; RRID: AB_2935797
Anti-ERK1/2 antibody	Santa Cruz Biotechnology	Cat# sc-514302; RRID: AB_2571739
Anti-phospho-ERK1/2	Santa Cruz Biotechnology	Cat# sc-136521; RRID: AB_10856869
Anti-phospho-p38 antibody	Santa Cruz Biotechnology	Cat# sc-166182; RRID: AB_2141746
Anti-p50 antibody	Santa Cruz Biotechnology	Cat# sc-8414; RRID: AB_628015
Anti-cleaved caspase 3 antibody	Abcam	Cat# ab13847; RRID: AB_443014
Anti-mouse IgG, HRP-linked Antibody	Cell Signaling Technology	Cat# 7076; RRID:AB_330924
Anti-rabbit IgG, HRP-linked Antibody	Cell Signaling Technology	Cat# 7074; RRID:AB_2099233
Anti-mouse IgG, AP-linked Antibody	Cell Signaling Technology	Cat# 7056; RRID:AB_330921
Anti-rabbit IgG, AP-linked Antibody	Cell Signaling Technology	Cat# 7054; RRID:AB_2099235
Anti-mouse IgG (H+L), F(ab')2 Fragment (Alexa Fluor® 488 Conjugate)	Cell Signaling Technology	Cat# 4408; RRID: AB_10694704
Anti-rabbit IgG (H+L), F(ab')2 Fragment (Alexa Fluor® 488 Conjugate)	Cell Signaling Technology	Cat# 4412; RRID: AB_1904025
Anti-rabbit IgG (H+L), F(ab')2 Fragment (Alexa Fluor® 555 Conjugate)	Cell Signaling Technology	Cat# 4413; RRID: AB_10694110
Anti-mouse IgG (H+L), F(ab')2 Fragment (Alexa Fluor® 555 Conjugate)	Cell Signaling Technology	Cat# 4409; RRID: AB_1904022
Veri Blot	Abcam	Cat# ab131366
Bacterial and virus strains		
Environmental bacterial isolates	salt farm of CSIR-CSMCRI, Bhavnagar (21° 47'50'' N, 72° 07'16'' E), Gujrat, India.	N/A
Chemicals		
JC-1 staining powder	Invitrogen™	Cat# T3168
2',7'-Dichlorodihydrofluorescein diacetate	Sigma	Cat# D6883
Mito tracker green FM	Invitrogen™	Cat# M7514
ML-161	Sigma	Cat# SML0418
SB203580	Sigma	Cat# 559389
MG132	Sigma	Cat# M7449

(*Continued on next page*)

Continued

REAGENT or RESOURCE	SOURCE	IDENTIFIER
DAPI	Sigma	Cat# D9542
Hoechst 33342	Invitrogen™	Cat# H21492
Lipofectamine™ 3000 transfection reagent	Invitrogen™	Cat# L3000001
Protein A agarose beads	Cell Signaling Technology	Cat# 9863S
Protein G agarose beads	Cell Signaling Technology	CST# 37478S
DEAE-52 matrix	Whatman	Cat# 4057050
Sephadex G-75 matrix	MP biomedical	Cat# 195589
DNA ladder	Invitrogen™	Cat# 15628050
Protein ladder	Abcam	Cat# ab116028
Protein ladder	G-bioscience	Cat# 786419
ECL substrate	Thermo scientific	Cat# 34580
BCIP/NBT substrate	Bio-rad	Cat# 1706432
Azocasein	Sigma	Cat# A2765
Ammonium sulphate	Sigma	Cat# A4915
Freund's complete adjuvant	Sigma	Cat# F5881
Freund's incomplete adjuvant	Sigma	Cat# F5506
GoTaq green master mix	Promega	Cat# M7122
SYBR green reagent	Eurogentec	Cat# UFRSMTBC101
MTT	Sigma	Cat# M5655
BCA assay kit	Thermo Scientific™	Cat# 23225
Annexin V and PI staining kit	BD	Cat# 556547
RNA isolation kit	Zymo research	Cat# R1057
Revertaid first strand cDNA synthesis kit	Thermo scientific	Cat# K1622
NE-PER™ Nuclear and Cytoplasmic Extraction kit	Thermo Scientific™	Cat#78833
Deposited data		
16s rRNA sequence of *Bacillus altitudinis* isolate GDL-186	This Paper	GenBank: OP738003.1
Whole genome sequence of *Bacillus altitudinis* isolate GDL-186	This Paper	GenBank : JAZHFY000000000.
Experimental models: Cell lines		
Human: PA-1	Gift from Dr. S.S.Roy, CSIR-IICB, Kolkata, India	ATCC, Cat# CRL-1572; RRID:CVCL_0479
Human: SKOV3	Gift from Dr. S.S.Roy, CSIR-IICB, Kolkata, India	ATCC, Cat# HTB-77; RRID:CVCL_0532
Human: IOSE 364	Gift from Dr. S.S.Roy, CSIR-IICB, Kolkata, India	RRID: CVCL_5540
Murine: ID8	Gift from Dr. S.S.Roy, CSIR-IICB, Kolkata, India	(MERCK Cat# SCC145; RRID: CVCL_IU14
Mouse peritoneal macrophage	Isolated in our lab	N/A
Experimental models: organisms/strains		
	India.	
C57BL/6 Female Mice	ICMR-NICED	N/A
New Zealand White Rabbit	ICMR-NICED	N/A
Oligonucleotides		
PAR-1 si-RNA	Eurogentec	N/A
Scrambled (SCR) siRNA	Santa Cruz Biotechnology	Cat#sc-37007
Primers for human PAR-1, PAR-2, PAR-3, PAR-4, GAPDH, Bacterial Peptidase M84, DNA gyrase B (Table S1)	Integrated DNA Technologies	N/A

(*Continued on next page*)

Continued

REAGENT or RESOURCE	SOURCE	IDENTIFIER
Software and algorithms		
ImageJ software	ImageJ	RRID: SCR_003070
BD FACS Aria II using 'Cell Quest' software	BD	RRID: SCR_014489
GelQuant	Thermo Fisher Scientific	N/A
Fiji	Image J	RRID: SCR_002285
Microsoft Office Excel 2021	Microsoft Windows	N/A
Adobe photoshop CS2	Adobe	N/A

RESOURCE AVAILABILITY

Lead contact

Information and requests for resources should be directed to and will be fulfilled by the lead contact, Dr. Amit Pal (pala.niced@gov.in/ palamit.app@gmail.com).

Materials availability

This study did not generate any new unique reagents.

Data and code availability

- Data: The data presented in this study are available in the article and supplemental information.
- Code: NCBI GenBank accession number of *Bacillus altitudinis* strain GDL-186 https://www.ncbi.nlm.nih.gov/nuccore/OP738003.1. The whole genome shotgun project of *Bacillus altitudinis* GDL 186 has been deposited at DDBJ/ENA/GenBank under the accession JAZHFY000000000. The version described in this paper is version JAZHFY010000000.
- Any additional information required to re-analyse the data reported in this paper is available from the lead contact upon request.
- The data presented in this study are available in the article and supplemental information. Any additional information required to re-analyse the data reported in this paper is available from the lead contact upon request.

EXPERIMENTAL MODEL AND STUDY PARTICIPANT DETAILS

Ethical approval for animal studies

All animal experiments were approved by the institutional animal ethics committee (IAEC), for animal care of National Institute of Cholera and Enteric Diseases (NICED), supplied with food pellets and autoclaved water *ad libitum*. The experimental design of the present study was approved by the Institutional Animal Ethics Committee (License No: PRO/168/Jan 2022), NICED, Kolkata, India.

Bacterial isolates and its growth conditions

A total of 200 bacterial isolates were isolated from salt farm of CSIR-CSMCRI, Bhavnagar (21° 47'50'' N, 72° 07'16'' E), Gujrat, India. All the isolates were stored in 25% glycerol at -80° C. Bacterial isolates were revived in nutrient broth (BD, USA; Cat# 234000) of pH 8.0 containing 2% NaCl (BD, USA; Cat# 234000). Initially, isolates were grown in 5.0 ml NB (primary culture) at 37° C in a shaker incubator till the OD_{600} reached 0.6. Secondary cultures were given in 1000 ml NB at a ratio of 1:100 and grown at 37° C in a shaker incubator for 18 h. The culture supernatant of the bacterial isolates was used for screening of protease.

Cell culture and treatments

Human ovarian cancer cells PA-1 (ATCC; Manassas, Virginia, United State; Cat# CRL-1572; RRID: CVCL_0479) and SKOV3 (ATCC; Manassas, Virginia, United State; Cat# HTB-77; RRID:CVCL_0532) were cultured (10-12 passage) and maintained in alpha-minimum essential medium (MEM-α) (Sigma; Cat# M0644) and RPMI-1640 (Gibco; Cat# 23400021) respectively with 10% FBS (Gibco; Cat# 10270106), 100 U/ml penicillin G and 100 μg/ml Streptomycin sulphate solution (Gibco, Cat # 15140122) at 37°C in presence of 5% CO_2 incubator. Human immortalised ovarian surface epithelial cells, IOSE (IOSE-364 from N. Auersperg and C. Salamanca, Vancouver, Canada, RRID: CVCL_5540) was maintained in MCDB-105 (Sigma Aldrich; Cat# M6395) and Medium-199 (Gibco; Cat# 31100035) in 1: 1 ratio and supplemented as stated earlier. Here, the low-passage cultures of human ovarian surface epithelium cells (isolated by scraping from human ovarian surface tissue) were immortalised by transfecting with SV40 large-T antigen viral particles.[73,74] Mouse ovarian carcinoma ID8 (MERCK Cat# SCC145; RRID: CVCL_IU14) cell line was cultured in DMEM high glucose medium (Gibco; Cat# 31600034) supplemented with 10% FBS, 100 U/ml penicillin G and 100 μg/ml Streptomycin sulphate and 1% AOF-ITS supplement (Merck; Cat# SCM 054) at 37°C in presence of 5% CO_2 incubator. All cell lines were supplied by

Dr. Sib Sankar Roy (CSIR-IICB, Kolkata) as a gift. Cell lines were tested for mycoplasma contamination and validated by short tandem repeat (STR) polymorphism analysis performed by the Life code genomic technologies.

Mice for animal model experiments

The mice that were used in this study were healthy adult female C57BL/6 mice of approximately 22–25 g of weight (6-8 weeks old), bred and maintained in an animal colony as per the principles and guidelines of the ethical committee for animal care of National Institute of Cholera and Enteric Diseases (NICED).

Rabbit for animal model experiments

Antiserum against Peptidase M84 was raised by immunizing an adult male New Zealand White rabbit (bred and maintained in an animal colony as per the principles and guidelines of the ethical committee for animal care of NICED.

METHOD DETAILS

Azocasein assay

Azocasein assay was performed to determine the protease activity of the bacterial isolates as described earlier (Syngkon et al., 2010).[75] Briefly, the overnight grown culture supernatants were mixed with 0.7% azocasein (prepared in 100 mM Tris-HCl; pH 8.0) (Sigma, Cat# A2765) followed by incubation at 37° C for 1 h. The reaction was stopped using 10% Tri Chloro Acetic Acid (Sigma; Cat# T6399) and kept at 4° C for 30 min. Precipitate was removed by centrifugation (12,000 rpm for 10 min). NaOH (500 mM) was added to the supernatant and absorbance was measured at 440 nm. Nutrient broth and purified haemagglutinin protease (HAP) from *Vibrio cholerae* C6709 were used as negative and positive controls respectively.

Purification and identification of protease

Peptidase M84 was purified from the culture supernatant of 'GDL-186'. Bacterial strain was grown in 1000 ml NB (containing 2% NaCl, pH 8.0) for 19 h at 37° C in a shaker incubator. After centrifugation at 12,000 rpm for 10 min at 4° C, the culture supernatant was salted out with 80% saturated ammonium sulphate (Sigma; Cat# A4915) and kept overnight (O/N) at 4° C. Protein pellet was collected by centrifugation at 14000 rpm at 4°C and the pellet was dissolved in 25 mM Tris-Cl buffer, pH 8.0. The protein solution was dialysed against the same buffer for 48 h at 4° C using dialysis membrane (Himedia; Cat# LA395-30MT). Dialysed protein solution was concentrated using speed-vac vacuum centrifugation and run on DEAE-52 ion-exchange column (2.5 X 20 cm) pre-equilibrated with 25 mM Tris-Cl buffer, pH 8.0. Flow through or non-binding fraction was collected, concentrated and checked for protease activity. Binding fractions were collected using increasing concentration of NaCl (0.1 M - 0.5 M) solution. The eluted fractions were pooled, dialysed, concentrated and examined for protease activity. Non-binding fraction showing protease activity, was further pooled, concentrated and loaded into Sephadex G-75 gel filtration column (1.5 X 30 cm) with 25 mM Tris-HCl buffer of pH 8.0. Fractions positive for protease activity were eluted, concentrated and analysed by SDS and Native-PAGE. The single band from Native-PAGE and two bands from SDS-PAGE were cut out from the gel and sent to C-CAMP, NCBS, Bangalore, India for identification by nano-LC-MS/MS-TOF. Peptide sequence generated from MS/MS spectra was searched in NCBI and Uniprot databases for homology alignment.

Determination of physico-chemical characteristics of the purified protease

Inhibition of the protease activity with different inhibitors was performed in order to determine the type of the purified protease and the culture supernatant of isolate GDL-186. PMSF (10 mM) (Sigma; Cat# P7626), EDTA (10 mM) (Sigma; Cat# E9884) and 1,10 phenanthroline (10 mM) (Sigma, Cat# 131377) were used in the inhibition study as described in our previous study (Tapader et al., 2016).[76] 100 mM stocks of PMSF and 1,10 phenanthroline were prepared in isopropanol and methanol respectively and 500 mM stock of EDTA was prepared in water. 5.0 μg of purified protease was pre-incubated at 37° C for 1 h with each inhibitor. The residual protease activity was measured by azocasein assay.

The optimum pH for protease activity was determined using buffers of different pH ranging from 4.0–11.0. 5.0 μg of purified protease was dialysed overnight against 25 mM acetate buffer (pH 4.0–5.0), 25 mM phosphate buffer (pH 6.0–7.0), 25 mM Tris-HCl (pH 8.0–9.0), 25 mM glycine-NaOH buffer (pH 10.0–11.0) and activity were determined with azocasein assay.

To determine the optimum temperature for activity, 5.0 μg of the purified protease was incubated over a wide range of temperatures: 4° C, 25° C, 37° C, 50° C, 60° C and 70° C for 1 h and the enzyme activity was determined by azocasein assay as already described.

Gelatine zymography was performed to determine the substrate specificity of the purified protease as per the protocol described earlier (Tapader et al., 2016).[41] For native zymography, samples were electrophoresed under non-reducing conditions without boiling using 7.5% Native-PAGE co-polymerised with 0.1% gelatin (Sigma; Cat# G2500). The gel was incubated after electrophoresis in renaturation buffer (2.5% Triton-X-100) for 1 h at room temperature (RT) with gentle shaking. The gel was then developed in development buffer containing 5 mM $CaCl_2$, 25 mM Tris-HCl (pH 8.0) for O/N at 37°C with gentle shaking. The gel was visualised after staining using Coomassie Brilliant Blue G-250 (Himedia; Cat# ML046) and subsequent destaining.

The effect of zinc ion (Zn^{2+}) or zinc dependency of the protease was also examined. The enzyme (5 μg) was preincubated with different concentrations of $ZnCl_2$ ranging from 0.5 mM to 15 mM at 37° C for 1 h. The azocaseinolytic activity was evaluated as described above.

16s-rRNA and whole genome sequencing

The protease positive bacterial isolate which showed significant apoptotic activity was identified by 16s rRNA sequencing. First, genomic DNA was isolated from O/N grown bacterial culture and run on 1.0% Agarose gel.16S rRNA gene was amplified by 27F 5′-AGAGTTT-GATCCTGGCTCAG-3′ and 1492R 5′-GGTTACCTTGTTACGACTT-3′ primers. The PCR reaction was as follows: 95° C for 10 min; 35 cycles of 95° C for 30 s, 55° C for 1 min, and 72° C for 1.5 min; and final extension at 72° C for 10 min. The PCR amplicon was purified to remove contaminants. Forward and reverse DNA sequencing reaction of PCR amplicon was carried out with forward primer and reverse primers using BDT v3.1 Cycle sequencing kit on ABI 3730xl Genetic Analyzer. The consensus sequence of 16S rRNA gene was generated from forward and reverse sequence data using aligner software. The 16S rRNA gene sequence was used to carry out BLAST with database of NCBI GenBank. Based on maximum identity score first ten sequences were selected and aligned using multiple alignment software program Clustal W. Distance matrix was generated and the phylogenetic tree was constructed using MEGA 7. The evolutionary history was inferred by using the Maximum Likelihood method based on the Kimura 2- parameter model. In addition to this, The DNA gyrase B gene sequence was used to carry out BLAST with database of NCBI GenBank. Based on maximum identity score first ten sequences were selected and aligned using multiple alignment software program Clustal W and NCBI. The evolutionary history was inferred by using the Neighbour joining method based on the Kimura 2- parameter model. Final confirmation of the isolate was validated by whole genome-based shotgun sequencing. Paired-end raw sequence reads were assessed for base quality and contamination by sequencing artefacts. Trimming of adapters and poor-quality sequences was performed for paired sequence reads with Trim Galore. Trimmed sequence reads were assembled into scaffolds with SPAdes. Taxonomic classification with Bracken and BLAST was used to identify closest genomic reference sequences. Sequences from draft genome assembly were mapped and ordered with RagTag. Annotation of assembled and ordered draft genome sequences was performed with Prokka. Genomic map plots were generated with Cgview from .gbk annotation file generatedby Prokka. Kraken2 and Bracken are used to align the filtered reads to prebuilt standard reference (archaea, bacteria, viral, plasmid, human, UniVec_Core).

Identification of the isolate based on biochemical, microbiological and physiological characteristics

Phenotypic characteristics of the isolate, including motility, cell morphology, Gram staining, catalase, and oxidase production, among others, were investigated according to standard protocols. The fermentation of substrate belonging to carbohydrates and derivatives was determined as per standard protocols.

Raising of antisera against purified Peptidase M84

Antiserum against Peptidase M84 was raised by immunizing a New Zealand White rabbit as described previously by Mondal et al., 2016.[77] Intramuscular injection was given with 100 μg of purified Peptidase M84 emulsified with an equal volume of Freund's complete adjuvant (Sigma, USA; Cat# F5881). This was followed by four booster injections with 100.0 μg of Peptidase M84 and incomplete adjuvant (Sigma, USA; Cat# F5506) at 7-day intervals. Blood samples were collected from rabbits on day 0 and 3rd day after the final injection and were allowed to clot O/N at RT. Sera were collected and centrifuged (1,000 rpm, 5 min), diluted in autoclaved glycerol (Sigma, USA) and stored at -80°C until use at a dilution of 1:800 unless otherwise mentioned.

PCR amplification to detect the gene encodes Peptidase M84 from *Bacillus altitudinis*

Genomic DNA was isolated from 1 ml of O/N bacterial culture using Promega Wizard genomic DNA purification kit (Cat# A1120) according to the manufacturer's protocol. 20 ng of genomic DNA was subjected to PCR amplification using GoTaq green master mix (Promega; Cat# M7122) in an automated thermal cycler (Bio-Rad, USA) to detect the presence of gene codes for Peptidase M84 using specific primers (mentioned in Table S1) under the following conditions: 10 min initial denaturation at 95°C followed by 35 cycles of 1 min denaturation at 95°C, 30 s, annealing at 55°C, followed by 1 min extension at 72°C and final 10 min extension at 72°C.

Cell viability and cell proliferation assay

The effect of Peptidase M84 on cellular viability and to determine the sub-lethal concentration of peptidase M84, MTT assay was done as per standard protocol (Kar et al., 2014).[78] About 1X10^5 live cells/well were seeded in a 96-well plate for viability assay. Trypan blue was used to determine cell viability. After 24 h of incubation, PA-1, SKOV3 and ID8 cells were treated with different concentrations of Peptidase M84 to determine the minimal inhibitory concentration (IC_{50}) value. After 24 h of protease treatment at different concentrations of 0.5 μg/ml – 5.0 μg/ml, MTT solution (0.8 mg/ml dissolved in serum free medium) was added to the cells and further incubated for 4 h in the dark at 37°C. The media containing MTT was removed and DMSO was added followed by incubation for 15 min in the dark. The absorbance was measured at 595 nm and mean of five replicates was taken to obtain IC_{50} value for subsequent experiments.

The effect of Peptidase M84 on cell viability was also studied by immunofluorescence of ki-67 nuclear antigen in PA-1 and SKOV3 cells. Peptidase M84 treated (with 2.0 μg/ml for 18 h) and untreated PA-1 and SKOV3 cells were fixed with 4 % paraformaldehyde for 10 min at RT. Cells were then permeabilised with 0.1 % Triton X-100 in 0.1% sodium citrate solution and blocked with 5% serum. Cells were incubated O/N with anti-ki-67 primary antibody (1:200) at 4°C in a moist chamber. Cells were washed with (phosphate buffer saline) PBS and then incubated with Alexa 488 conjugated secondary antibody. Nuclei were stained with DAPI for 10 min at 37°C. Cells were then washed twice with PBS, mounting was done with 10% glycerol. Images were captured using Zeiss (LSM 710) confocal microscope.

Flow cytometry analysis to study apoptosis

Flow cytometry was performed for screening of apoptotic activity of protease positive bacterial culture supernatants. Cellular apoptosis was detected by double staining, FITC conjugated annexinV/propidium iodide (PI) staining, as described in our previous studies (Ray et al., 2016).[27] Briefly, PA-1 cells (1×10^6) were seeded into 6 well tissue culture plates. Cells with 70% confluency were washed with PBS and starved in serum free media for 18 h. Cells were treated with filter sterilised protease positive bacterial supernatant for 18 h in complete medium. Untreated control cells were replaced with fresh media and incubated under similar conditions. After treatment, cells were harvested and flow cytometric analysis was done by using Annexin V and PI staining kit (BD, USA, Cat# 556547) as per the manufacturer's protocol. For protease inhibition studies bacterial culture supernatant was pre-incubated with both 10 mM EDTA and 10 mM PMSF before treatment.

Flow cytometry was also performed with the purified protease as described below. After treatment with purified Peptidase M84 at a concentration range between 1.0 μg/ml to 3.0 μg/ml for 18 h, PA-1, SKOV3, IOSE and ID8 cells were harvested by centrifugation and washed twice with PBS. Cells were re-suspended in 1X binding buffer (provided with BD annexin-V kit), stained with annexin V/PI and kept at RT for 15 mins. Cells were analysed by BD FACS Aria II using 'Cell Quest' software. For protease inhibition studies, Peptidase M84 was preincubated with either 10 mM EDTA or 10 mM PMSF before treatment.

Chromatin condensation assay

After treatment with 2.0 μg/ml of protease for 18 h, ovarian cancer cells were stained with Hoechst 33342 stain (2 μg/ml) and incubated for 10 min at 37°C, and images were taken under Zeiss confocal microscope. Condensed nucleus was counted against total number of nuclei in the field, and the percentage of apoptotic nuclei were calculated and plotted graphically.[42]

Isolation of peritoneal exudate macrophages (PEMΦ) and treatment

To assess the cytotoxic effects of purified protease on normal healthy cells of mice the peritoneal exudate macrophages (PEMΦ) were isolated from 6-8 weeks of old C57BL/6 female mice as described previously (Chakraborty and Bhaumik, 2020; Naskar et al., 2014).[79,80] Briefly, Naive C57BL/6 mice were injected intraperitoneally once with 3.0 ml of a 4% (w/v) starch (Sigma, USA) solution. After 48 h, PEMΦ were collected by peritoneal washing with chilled PBS followed by centrifugation of the exudate and resuspension of cell pellet in RPMI-1640 medium supplemented with 10% FBS (Gibco, USA), 100 U penicillin/ml, and 100 μg streptomycin/ml (Gibco, USA). Cells were then seeded into 6-well plates at $5X10^4$ cells/ml. The cells were then cultured for 48 h at 37°C in a humidified 5% CO_2 incubator to dampen any residual effects of the starch. Non-adherent cells were removed thereafter by gentle washing with serum-free medium. The remaining adherent cells were treated with 3.0 μg/ml of Peptidase M84 for 18 h. The untreated and treated cells were collected by gentle scraping for use in the FITC conjugated annexin V/ (PI) dual staining-based apoptosis detection assay by flow cytometry as per the protocol described earlier.

Detection of ROS by DCFDA staining

In-situ ROS level was measured by oxidation of 2′,7′- dichlorofluorescin diacetate (DCFDA) to highly fluorescent 2′,7′-dichlorofluorescin (DCF). Peptidase M84 treated (2.0 μg/ml) PA-1, SKOV3, IOSE cells and ID8 (3.0 μg/ml) cells for 6 h and 18 h with their respective untreated controls were incubated with DCFDA at a working concentration of 20 μM for 20 min at 37°C, washed with PBS and subsequently the cell pellet was resuspended in 500 μl of PBS and then subjected to flow cytometry and analysed by BD FACS Aria II using 'Cell Quest' software. At least three independent experiments were conducted to validate our results and the mean fluorescence intensity value of DCF was plotted for quantification.

Flow cytometry detection of JC-1 fluorescence

JC-1 dye (Invitrogen, USA) staining to detect changes in mitochondrial membrane potential in ovarian cancer cells was done according to the protocol described by Prasad et al., 2021.[81] Briefly, PA-1 and SKOV3 cells ($1X10^6$) were harvested by centrifugation (5 min at 500×g) after Peptidase M84 treatment (2.0 μg/ml for 6 h and 18 h). Cells were then resuspended in 500 μl of PBS. JC-1 (5,50,6,60-tetrachloro-1,10,3,30-tetraethylimidacarbocyanine iodide) was added to a final concentration of 10.0 μg/ml from a stock solution of 5.0 mg/ml and cells were incubated in dark at 37°C for 30 min. Cells were then washed once and again resuspended in 500 μl of PBS. Cells were analysed in a BD FACS Aria II flow cytometer (BD Bioscience, San Jose, CA, USA). The ratio of the median value of green and red fluorescence was plotted for quantification.

Comet assay

DNA damage (single strand breaks) was measured by alkaline comet assay (Singh et al., 1988).[82] Briefly, PA-1 and SKOV3 control and Peptidase M84 treated (2.0 μg/ml for 18 h) cells were suspended in 0.6% (w/v) low melting agarose. Subsequently, cells were layered over a frosted microscopic slide previously coated with a layer of 0.75% normal melting agarose. The slides were then immersed in a lysis buffer of pH 10.0 and left overnight at 4°C. Slides were transferred into a horizontal electrophoresis chamber containing an alkaline solution (300 mM NaOH, 1 mM Na_2EDTA; pH 13.0). Pre-soaking for 20 min was done in order to unwind DNA. Electrophoresis was then carried out for 20 min (300 mA, 20 V). Slides were washed thrice with neutralizing buffer (Tris Buffer 0.4 M, pH 7.5) followed by staining with ethidium bromide (final concentration 40.0 μg/ml). Slides were examined under Axio observer 7 Apotome.2; objective-EC Plan-Neofluar 40X / 0.75 NA fluorescence microscope and image analysis was done using comet assay software programme Komet 5.5. DNA damage was quantitated by tail moment measurement.

Western blotting (WB)

Western blot was done as described by Ray et al., 2016; Das et al., 2022.[27,83] Briefly, cultured cells were lysed with RIPA buffer and the concentration of protein samples was measured using BCA assay kit. Equal amount of protein was loaded onto SDS-PAGE for separation and then electrophoretically transferred to the PVDF membrane (Merck; Cat# IPVH00010). After transfer the membrane was blocked with 3% BSA (Sigma; Cat# A1470) in Tris-buffered-saline (TBS) and incubated overnight with primary antibody (1: 1000) against the protein of interest (as per requirement) at 4°C. The blot was washed with TBS-Twin 20 (TBST) buffer and incubated with HRP/AP-tagged secondary antibody for 2 h at RT. Proteins were either visualized by Bio-Rad gel documentation system using specific ECL substrate (Thermo scientific; Cat# 34580) for HRP tagged antibodies (Cell Signaling Technology Cat# 7076 and Cell Signaling Technology Cat# 7074) or using BCIP/NBT substrate (Bio-rad; Cat# 1706432) for AP tagged antibodies (Cell Signaling Technology Cat# 7056 and Cell Signaling Technology Cat# 7054). Quantification of western blots was performed using GelQuant (Thermo Fisher Scientific, USA) and ImageJ (NIH, Bethesda, MD) software. At least three independent experiments were performed to confirm the findings and band intensities were normalised to loading controls.

Immunocytochemistry and confocal imaging

Peptidase M84 treated (2.0 μg/ml for 18 h) and untreated PA-1 and SKOV3 cells were fixed with 4% paraformaldehyde for 10 min at RT. Cells were then permeabilized with 0.1 % Triton X-100 in 0.1% sodium citrate solution and blocked with 5% FBS. Cells were incubated O/N with primary antibody (1:200) against the protein of interest (as per requirement) at 4°C in a moist chamber. Cells were washed with PBS and incubated with either Alexa 488 (Cell Signaling Technology Cat# 4408 and Cell Signaling Technology Cat# 4412) or Alexa 555 conjugated secondary antibody (Cell Signaling Technology Cat# 4413 and Cell Signaling Technology Cat# 4409) for 2 h at RT. Nuclei were stained with either DAPI or Hoechst 33342 (working concentration 1.0 μg/ml) for 10 min at 37°C. Cells were washed twice and mounting was done with 10% glycerol. Images were captured using confocal microscope (Zeiss 710); objective-Plan-Apochromat 63X / 1.40 NA. c and all the other required analysis was done according to the procedure described by Das et al., 2022.[83]

Evaluation of intracellular cytochrome c by western blot and immunofluorescence

Subcellular fractionation to extract mitochondria free cytosol from PA-1 and SKOV3 cell lysates was performed. using the method described by Dimauro et al. 2012.[84] Briefly, $5x10^6$ cells were harvested after 18 h of protease treatment (2.0 μg/ml) by trypsinisation followed by the isolation of mitochondria free cytosolic fraction to assess the release of cytochrome c. Concentration of cytochrome c in cytosolic fraction was measured by western blot in protease treated and untreated cells. Cytosolic GAPDH (mitochondria free) was used as loading control.

To observe the intracellular cytochrome c distribution, co-localization-based immunofluorescence was used as described earlier (Li et al., 2020; Sun et al., 2008).[85,86] Briefly, PA-1 and SKOV3 cells were treated with Peptidase M84 for 18 h at a concentration of 2.0 μg/ml. Untreated and treated cells were incubated with Mito Tracker dye (Mito Tracker Green FM; Molecular Probes; Thermo Fisher Scientific) at a working concentration of 100 nm for 40 min in a 37°C incubator in dark. The slides were then fixed with 4% formaldehyde at RT for 15 min. The fixed slides were stained with anti-cytochrome c antibody (1:200) and kept O/N at 4°C in a moist chamber, followed by staining with Alexa 555 labelled secondary antibody (1:200) at RT for 2 h. Cells were stained with DAPI (1.0 μg/ml) for 10 min, washed twice and mounted with 10% glycerol in glass slides. Images were obtained using different excitation filters and merged. Co-localisation was quantified by calculating Pearson's co-efficient values.

RT-qPCR

RT-qPCR of PARs was done as described previously (Ray and Pal, 2016).[37] Total cellular RNA was isolated from untreated and Peptidase M84 treated (2.0 μg/ml for 18 h) PA-1 and SKOV3 cells (about 1X 10^6 cells for PA1 and $0.8X10^6$ cells for SKOV3) using RNA isolation kit (Zymo research; Cat# R1057). 2.0 μg of the total RNA was reverse transcribed using Revertaid first strand cDNA synthesis kit (Thermo scientific; Cat# K1622) to synthesize the cDNA first strand. Thereafter, the cDNA first strand was used in the subsequent amplification by Real-Time PCR with the primers described in Table S1. GAPDH was used as an internal control to normalize the results. Real-Time PCR was performed using SYBR green reagent (Eurogentec; Cat# UFRSMTBC101) in a total volume of 25 μl containing 10 pM of each primer (mentioned in Table S1), 12.5 μl of SYBR green reagent and 2.0 μl of cDNA. PCR reactions were carried out by using an ABI multicolour real time PCR detection system. The thermal cycling conditions used for Real Time PCR were: denaturation at 95°C for 30 s followed by 35 cycles of 1 min denaturation at 95°C, 30 s, annealing at 55°C, followed by 1 min extension at 72°C and final 10 min extension at 72°C.

Immunoprecipitation

For immunoprecipitation (IP), cells were lysed in immunoprecipitation buffer [50 mM Tris-HCl, pH 7.5, 150 mM NaCl, 0.1% Triton X-100, 1% IGEPAL and 1 mM PMSF], and it was performed under denaturing conditions as described previously by Ray and Pal, 2016.[37] Briefly, 2.0 μg/ml of Peptidase M84 was added to the PA-1 and SKOV3 cell medium and incubated for 30 min. The incubation media was removed after centrifugation and cells were fixed with 4% formaldehyde and the cell lysate was prepared using RIPA buffer. 500 μg of the total lysate was incubated with either PAR-1 antibody or antisera raised against Peptidase M84 for 5 h at 4°C in a rotating shaker at a speed of 10 rpm. The lysate along with antibody was allowed to bind with A/G agarose beads and incubated O/N at 4°C in a rotating shaker at a speed of 10 rpm. The lysates were centrifuged and washed twice with IP buffer to remove any non-specific bindings. Beads were boiled with SDS-protein loading dye for 10 min and subjected to electrophoresis. The proteins were transferred to a PVDF membrane and western blot was done with either

anti-Peptidase M84 antibody (1:3000) or anti-PAR-1 antibody (1:1000). Immunoblots (IB) were developed using Veri Blot (Abcam Cat# ab131366) as per the manufacturer's instruction to observe the interaction between Peptidase M84 and PAR-1.

Nuclear cytosolic fractionation

To detect the nuclear translocation of NFκB subunits, PA-1 and SKOV3 ($5X10^6$) cells were treated with 2.0 μg/ml of Peptidase M84 for 18 h. Extraction of nuclear and cytosolic fractions of untreated and Peptidase M84 treated cells were performed using NE-PER™ Nuclear and Cytoplasmic Extraction Reagents (Thermo Scientific™, USA, Cat#78833) according to manufacturer's protocol. The fractions were used for western blotting to determine nuclear translocation of p50 and p65. Here, α-tubulin and Histone H3 were used as cytosolic and nuclear loading controls respectively.

Treatments of cells and siRNA transfection

The cells were first starved for at least 18 h with an incomplete medium prior to respective treatments. Scrambled (SCR) siRNA (Cat#sc-37007, Santa Cruz Biotechnology) was used as control for knockdown studies. Lipofectamine 3000 was used as transfection reagent and transfection was performed according manufacturer's protocol. The transfection was done at 50–60% confluency and the transfection reagents were added in Opti-MEM (Gibco, USA; Cat# 31985062). medium and after 4 h of transfection the media was changed to respective media of treatment. PAR-1 si-RNA (CGGUCUGUUAUGUGUCUAUdTdT) was transfected for at least 48 hours for efficient knock down.

Flowcytometric analysis for apoptosis and ROS detection using inhibitors

Quantitative evaluation of apoptosis and ROS was performed using the flow cytometry methods as described previously by Ray and Pal, 2016.[37] PA-1 and SKOV3 cells ($1X10^6$ cells) were incubated with either 2.0 μg/ml of Peptidase M84 or pre-incubated for 1 h with 0.5 μM PAR1 inhibitor (ML161) or 3.0 μM of NFκB inhibitor (MG132), or 10.0 μM p38 inhibitor (SB203580) and then incubated with 2.0 μg /ml of Peptidase M84 for 18 h. Cells were washed with PBS and analysed to detect apoptosis by Annexin-V-FITC and PI dual staining based method. In-situ ROS was determined by DCFDA staining using FACS Aria II (Cell Quest software) as per the protocol described earlier.

Animal model

Survival kinetics and body weight changes were studied by implanting $5X10^6$ number of ID8 cells (0.2 ml) into the peritoneal cavity of C57BL/6 female mice and allowed to multiply.[71,72] The day of tumour implantation was assigned as day '0'. In the present study, the animals were randomised into six groups containing ten animals (n = 10) in each group. (i) **Group 1** normal set (non-tumour-bearing; untreated control); (ii) **Group 2** only tumour-bearing set (ID8 control); (iii) **Group 3** Peptidase M84-treated ID8 bearing set; where 3.0 μg /ml Peptidase M84 (12.0 μg / kg of body weight) was injected intraperitonially on the day after inoculation of ID8 cells and injected once in a week for seven successive weeks; (iv) **Group 4** Peptidase M84 pre-treated with 10 mM EDTA; tumour bearing set where Peptidase M84 was inhibited with 10 mM EDTA at 37°C for 1 h and then injected into the peritoneum cavity of ID8 treated mouse for seven successive weeks (v) **Group 5** Only Buffer treated set (vehicle control) where 100 μl of 1X PBS buffer was injected intraperitonially once in a week for seven successive weeks. (vi) **Group 6** only Peptidase M84 treated group (protease control).

The life span of each group of mice was evaluated by measuring the percentage of survival rate in each group at 10 days interval by using a formula:

(Number of live animals in a group/number of initial animals in that group) X100.

Collection of blood and serum samples

Blood samples from mice were collected as per the protocol reported previously (Barua et al., 2019).[87] Before euthanasia, all animals were fasted for 4 h then the blood samples were collected by cardiac puncture into microcentrifuge tubes and left to clot. The serum was separated by centrifugation at 2000 X g for 15 min and stored at -20°C until analysis.

Measurement of cellular ROS and liver and kidney toxicity in mice

Cellular ROS level was detected by biochemical analysis of different markers in serum samples of all groups of experimental mice as described above. Different biochemical parameters like lipid peroxidation (LPO), reduced glutathione (GSH), catalase (CAT) and superoxide dismutase (SOD) were measured in the serum of different groups of mice at day 0- and 45-days intervals after inoculation of cells using standard protocols as described earlier by Ray et al., 2016.[27]

Liver toxicity markers such as serum aspartate transaminase (AST), alanine aminotransferase (ALT) level and kidney toxicity markers such as urea and creatinine were analysed by automated clinical chemistry analyzer (AU400, Olympus, Japan) according to the manufacturer's protocol after 45 days of treatment.

Histology of liver and kidney tissue of mice

Histopathology and hematoxylin-eosin (HandE) staining of liver and kidney tissue was done as per protocol suggested by Dasgupta et al., 2022.[88] For the experimental purpose, euthanasia was done as per CPCSEA guidelines. The liver and kidney were harvested from all six

groups of mice mentioned earlier after 45 days of tumour implantation. The tissues were fixed in 10 % buffered formalin. The fixed tissue was paraffin embedded and serially sectioned at 4.0 μm, and stained with hematoxylin and eosin (H&E). Tissue Sections were viewed under 40X magnification of Zeiss Axiovert 40 C microscope.

In vivo evaluation of cell viability

The effects of 3.0 μg/ml of Peptidase M84 were compared against control groups, where mice were randomised in six different groups as mentioned earlier. After 45 days and 60 days of tumour inoculation, mice were sacrificed to collect total cells from the peritoneum and cells viability was checked by trypan blue exclusion method as described previously by Barua et al., 2020.[89]

Statistical analysis

All experiments were replicated at least thrice (n=3). All animal experimental groups contained either 10 or 6 animals. The experimental results were expressed as mean ± standard deviation. All statistical analysis was done by applying Student's t-test (unpaired two-tailed) and bar graphs were plotted using Microsoft Office Excel 2021. In all panels, ns (non-significant) $p>0.05$, *$p \leq 0.05$, **$p \leq 0.01$, and ***$p \leq 0.001$. In each panel, error bars were calculated based on results obtained from a minimum of three independent experiments.